



Final Report

Design and Evaluation of an Arterial-Friendly Local Ramp Metering System-Phase I: System Enhancements for Real-time Operations

Gang-Len Chang

University of Maryland, College Park

Email: gang@umd.edu

Yao Cheng

University of Maryland, College Park

Email: ycheng09@umd.edu

Date

September 2024

ACKNOWLEDGMENT

This research was supported by the Sustainable Mobility and Accessibility Regional Transportation Equity Research Center at Morgan State University and the University Transportation Center(s) Program of the U.S. Department of Transportation.

Disclaimer

The contents of this report reflect the views of the authors, who are responsible for the facts and the accuracy of the information presented herein. This document is disseminated in the interest of information exchange. The report is funded, partially or entirely, under grant number 69A3552348303 from the U.S. Department of Transportation's University Transportation Centers Program. The U.S. Government assumes no liability for the contents or use thereof.

©Morgan State University, 2024. Non-exclusive rights are retained by the U.S. DOT.

1. Report No. SM11	2. Government Accession No.	3. Recipient's Catalog No.	
4. Title and Subtitle Design and Evaluation of an Arterial-Friendly Local Ramp Metering System-Phase I: System Enhancements for Real-time Operations		5. Report Date August 2024	
		6. Performing Organization Code	
7. Author(s) Gang-Len Chang Yao Cheng		8. Performing Organization Report No.	
9. Performing Organization Name and Address University of Pittsburgh 4200 Fifth Ave, Pittsburgh, PA 15260		10. Work Unit No.	
		11. Contract or Grant No. 69A3552348303	
12. Sponsoring Agency Name and Address US Department of Transportation Office of the Secretary-Research UTC Program, RDT-30 1200 New Jersey Ave., SE Washington, DC 20590		13. Type of Report and Period Covered Final, September 2023 – August 2024	
		14. Sponsoring Agency Code	
15. Supplementary Notes			
16. Abstract This project investigates the development and evaluation of an Arterial-Friendly Ramp (AF-Ramp) metering system to optimize freeway and arterial traffic flow near freeway on-ramps. The AF-Ramp system integrates real-time data to coordinate ramp metering and intersection signal plans within the ramp impact area. Its primary goal is to mitigate common traffic issues such as on-ramp queue spillbacks and freeway congestion by optimizing ramp metering rates and local traffic signals in unison. This report, focusing on Phase I of the project, documents the system's enhancements for real-time operation and presents preliminary findings from simulations comparing the AF-Ramp system with conventional ramp metering models like ALINEA/Q. Results demonstrate the AF-Ramp system's superior performance in maintaining throughput and minimizing congestion in various traffic scenarios. Key contributions include introducing a lane-group-based macroscopic traffic prediction model and a comprehensive control mechanism integrating freeway ramp and arterial signal coordination.			
17. Key Words: traffic signals, e-commerce delivery, priority system, socially responsible system		18. Distribution Statement	
19. Security Classif. (of this report): Unclassified	20. Security Classif. (of this page) Unclassified	21. No. of Pages 42	22. Price

Chapter 1 Introduction

1.1 Background

To address on-ramp controls' negative impacts (e.g., ramp queue spillover) on neighboring arterials' traffic conditions, the research team has developed an innovative Arterial-Friendly Ramp (AF-Ramp) metering system. This system aims to maximize the efficiency of freeway and arterial users by optimizing ramp metering rates and coordinated signal plans for intersections within the ramp-impact area. Different from current ramp-metering models in the literature and in practice, the proposed AF-Ramp system includes the target freeway segment, its on-ramp, and neighboring intersections in one integrated control environment. In doing so, the ramp system's components stop competing for available roadway capacity and instead coordinate to maximize overall benefits.

Given the time-varying traffic patterns on both the freeway and its neighboring arterials, which fluctuate significantly during peak hours and congestion transition periods, a natural extension for the AF-Ramp system would be to advance its capabilities for real-time operations. This enhancement would utilize available traffic surveillance information, including detectors, and speed data from probe vehicles. Such a real-time version of AF-Ramp could then serve as the foundation for the full-scale development of real-time coordinated corridor control for congested segments, encompassing multiple on- and off-ramps as well as nearly saturated local intersections.

To ensure the AF-Ramp system's effectiveness in addressing complex, local-specific traffic patterns, it is essential that a rigorous and extensive field evaluation be conducted with respect to the system's key model parameters and embedded assumptions. The relationship between the system's three primary models, from estimating the freeway's remaining capacity for ramp flows to the optimization of ramp metering rates and intersection signal plans, can also be assessed with field data.

Note that the field evaluation of the developed AF-Ramp system shall include its performance in both off-line and real-time operations. Detection of any potential technical issues that may degrade the effectiveness of the developed system in real-time operations should also be investigated in field studies.

1.2 Objectives

The tasks to complete the development of the AF-Ramp include (1) system enhancements for real-time operations and (2) extensive performance evaluation with field data. Unfortunately, due to the lack of quality detector data over the statewide freeway networks, this project phase has focused mainly on the former subject. A preliminary design plan proposed for system performance evaluation with field data has also been included along with a discussion of technical extensions for the corridors with multi-ramp and multi-intersection real-time controls.

1.3 Report organization

All research results from the Phase-I study are organized into four chapters in this report. A brief description of primary focus and key findings documented in each chapter is summarized below:

Chapter 2 presents an overview of the time-of-day Arterial-Friendly local ramp metering control (AF-ramp) system for freeway operations by Cheng and Chang (2021). Such a system is designed to balance the benefits between freeway and arterial users and also to prevent on-ramp

queue spillbacks during recurrent congestion. Its core includes a lane-group-based macroscopic traffic module for predicting traffic states in real time and for executing control strategies aimed at maximizing the total throughput with coordinated operations between the ramp meter and nearby local intersection signals. Also reported in this chapter are the results of performance evaluations. Extensive simulation experiments have confirmed that the AF-ramp can outperform the widely applied real-time ramp control model, ALINEA/Q, under various experimental traffic scenarios.

The preliminary findings summarized in this chapter suggest that a real-time arterial-friendly ramp-metering system that considers both time-varying traffic dynamics and the concerns of local traffic users may serve as an effective and deployable strategy to contend with bottlenecks at freeway interchanges.

Chapter 3 provides a detailed discussion of the extended version of the AF-ramp system, which controls the entire interchange—including the on-ramp, off-ramp, and freeway mainline—to address recurrent congestion patterns on major freeway corridors. These congestion patterns frequently occur on a freeway interchange's on-ramp and off-ramp segments, where both exiting and merging flows often trigger a series of lane changes. This results in significant freeway speed reduction and the propagation of traffic queues onto neighboring surface streets.

The extended AF-ramp presented in this chapter is an Integrated Real-time Interchange Control (IRIC) system, which maximizes the benefit of both freeway and arterial users by fusing an integrated off-ramp signal control (IOSC) module, an off-ramp queue impact (OQI) model, a lane-group-based (LGB) traffic model, a ramp metering control strategy, and arterial signal optimization modules. Such an enhanced system with both ramp metering and local arterial signal functions can determine whether to implement system-wide optimization or solely ramp metering based on real-time detected traffic conditions. The evaluation results from simulation experiments have confirmed the effectiveness of the developed real-time interchange control system, especially with respect to its effectiveness in preventing ramp queue overflows onto neighboring arterials and minimizing the off-ramp spillback onto the freeway mainline.

Chapter 4 reports the proposed work for next phase, which is an experimental plan to evaluate the AF-ramp and its extension system, including: (1) conducting the field evaluation and refinement of the AF-Ramp system; and (2) streamlining the system's control configuration and its parameter updating procedures for convenient field implementation. More specifically, the focus of conducting an extensive field test includes evaluating the accuracy and reliability of the following three models embedded in the AF-Ramp system with field data from the System 1 highway network and performing necessary enhancements to facilitate its deployment in practice.

The entire plan for model assessment with field data consists of three phases, where phase-I is to evaluate the system's freeway traffic monitoring function for detecting the freeway flow rate upstream of an on-ramp, and for estimating the remaining capacity for on-ramp flows. Phase-II activities assess the effectiveness of integrating signal and ramp metering controls to concurrently optimize both the ramp metering rate and the signal timings at neighboring intersections. The last phase of the field evaluation plan is to ensure that the system's function for coordinating all intersections' turning movements heading to the on-ramp will not generate excessive queues.

Chapter 2 A Real-time Arterial-Friendly Ramp Metering (RAF-ramp) System

2.1 Background

To balance the benefits (or costs) between the freeway and arterial users in contending with recurrent local congestion, Cheng and Chang (2021) have developed an arterial-friendly local ramp metering control system for time-of-day and off-line operations. This study is to enhance their off-line system with a lane-group-based macroscopic traffic prediction module for real-time operations at freeway interchanges experiencing highly fluctuating traffic demands during peak hours.

In view of the literature, most existing models on local ramp control are operated in either fixed-time or traffic-responsive mode, depending on the availability of real-time traffic information. First put into practice in Chicago, IL in 1963 (Piotrowicz and Robinson, 1995), the fixed-time ramp metering control has since been deployed in several metropolitan areas (Los Angeles, CA, 1968; Minneapolis-St. Paul, MN, 1970; Seattle, WA, 1981; Denver, CO, 1981; Portland, OR, 1981; Detroit, MI, 1984). However, the core logic of such control with pre-determined metering rates on a time-of-day basis often fails to achieve the desired level of performance when traffic volumes significantly deviate from the historical patterns. Recognizing such deficiencies, several researchers proposed various traffic-responsive local metering control strategies (Masher et al., 1975; Papageorgiou et al., 1991; Papageorgiou et al., 1997; Zhang and Ritchie, 1997; Smaragdis and Papageorgiou, 2003; Xu et al., 2006; Hou et al., 2008) to contend with the time-varying traffic volume. Among them, ALINEA (Papageorgiou et al., 1991; Papageorgiou et al., 1997), a local feedback control ramp metering control strategy, is the most widely referenced. The ramp metering rates under such control are determined based on the difference between the observed occupancies downstream of the on-ramp segment and a preset critical value pre-calibrated from historical data. Recognizing that those local ramp metering strategies may not yield the desired level of effectiveness when the traffic bottleneck expands over multiple ramps, traffic researchers have further developed various multi-ramp coordinated control strategies for systemwide congestion control (Paesani, 1997; Papageorgiou et al., 1990; Papamichail et al., 2010; Wattleworth, 1965; Wang et al., 2008; Lipp et al., 1991; Liu et al., 1994; Shaaban et al., 2016).

All aforementioned strategies, despite their significant contributions to freeway congestion control, often face resistance from local traffic agencies and nearby arterial users when they come to field deployment. This is because such strategies with the control objective of improving traffic conditions on the freeway often incur excessive ramp vehicle queues and spillback to block local traffic (Wu et al., 2018; Zhang et al., 2001; Kattan and Saidi, 2011). Such concerns have mostly been addressed by restricting the metering rate with so-called queue-override functions (Smaragdis and Papageorgiou, 2003; (Paesani, 1997; Papamichail et al., 2010; Gordon, 1996; Sun and Horowitz, 2005). However, since locations that justify the implementation of ramp metering control are likely to experience high traffic volumes on both the freeway and its on-ramp, queue override functions may be frequently triggered by detectors, thus significantly degrading the effectiveness of metering controls.

To address such negative impacts on local traffic, some limited studies in the literature further included local intersections near the on-ramp in the control area so that nearby traffic signals can better coordinate with the ramp metering control (Head and Mirchandani, 1997; Tian et al., 2005; Tian, 2007; Su et al., 2014). Nevertheless, such control systems still place the freeway's

performance as their primary control objective with insufficient attention to the concerns often raised by local traffic users. To balance the benefits between the freeway and arterial users within a congested on-ramp area, Cheng and Chang (2021) have designed an Arterial-Friendly Local Ramp metering (named *AF-ramp*) control strategy to concurrently optimize the ramp metering rate and signal plans at those intersections feeding traffic to a freeway's on-ramp under time-of-day and off-line operations.

As a natural extension for the off-line AF-ramp model, this study proposes a Real-time Arterial-Friendly Ramp metering (RAF-ramp) system which aims to maximize total throughput while preventing on-ramp spillovers with optimized signal controls for its intersections. More specifically, an RAF-ramp with the function of concurrently optimizing ramp metering rates and signal plans at nearby intersections can effectively prevent not only on-ramp queue from spilling back to local intersections but also arterial link spillovers caused by excessive traffic volumes turning to the ramps during peak periods. Recognizing the discrepancy in the dynamic nature between ramp metering and signal controls, the RAF-ramp system has been embodied with a traffic-state monitoring mechanism that will trigger the concurrent optimization of both controls when justified to do so. Otherwise, the system will let the ramp metering dynamically adjust its metering rate under the optimized local signal control environment. Such a real-time arterial-friendly system, considering both the time-varying traffic dynamics and the loudly-voiced concerns of local traffic users, may well serve as an effective and deployable strategy to contend with the bottleneck at freeway interchanges. The key system features of the proposed RAF-RM system are to:

- Respond to time-varying traffic volumes on both the freeway and its neighboring arterial in a timely manner with proactive ramp and signal controls, based on the embedded lane-group-based traffic predicting module;
- Embody a traffic-state monitoring mechanism to govern the optimal timings for implementing either the dynamic metering cycles alone or a system-wide update to concurrently reoptimize signal plans for all nearby intersections;
- Maximize the total throughput for both the freeway and arterial links within the control area based on the real-time detected flows;
- Prevent ramp queues from spilling back to neighboring local streets by coordinating intersection signal plans with ramp metering control;
- Optimize the signal plan, including the cycle length, green splits, and phase sequences, for each nearby intersection to ensure that the traffic flows heading towards the on-ramp will not cause turning bay spillover; and
- Provide local progression for all path-flows within the control area of the local arterial with a set of specially designed offsets to avoid local arterial bottlenecks.

2.2 System structure for real-time controls

Figure 2.1 shows the operational flowchart of the proposed RAF-ramp system and its principal components, where the entire control process consists of the following three main stages: 1) system initialization and assessment, 2) projection of traffic evolution pattern and selection of the initial ramp metering cycle, and 3) dynamic execution of the integrated ramp and local signal controls based on predicted traffic conditions with the embedded Lane-Group-Based (LGB) model (26) and the system-wide optimization module for concurrent updates of ramp metering cycles and neighboring signal plans.

The control boundaries for such a system and the locations of vehicle detectors for real-time traffic monitoring and performance assessment are shown in Figure 2.2. A brief description of key activities at each control stage is presented below:

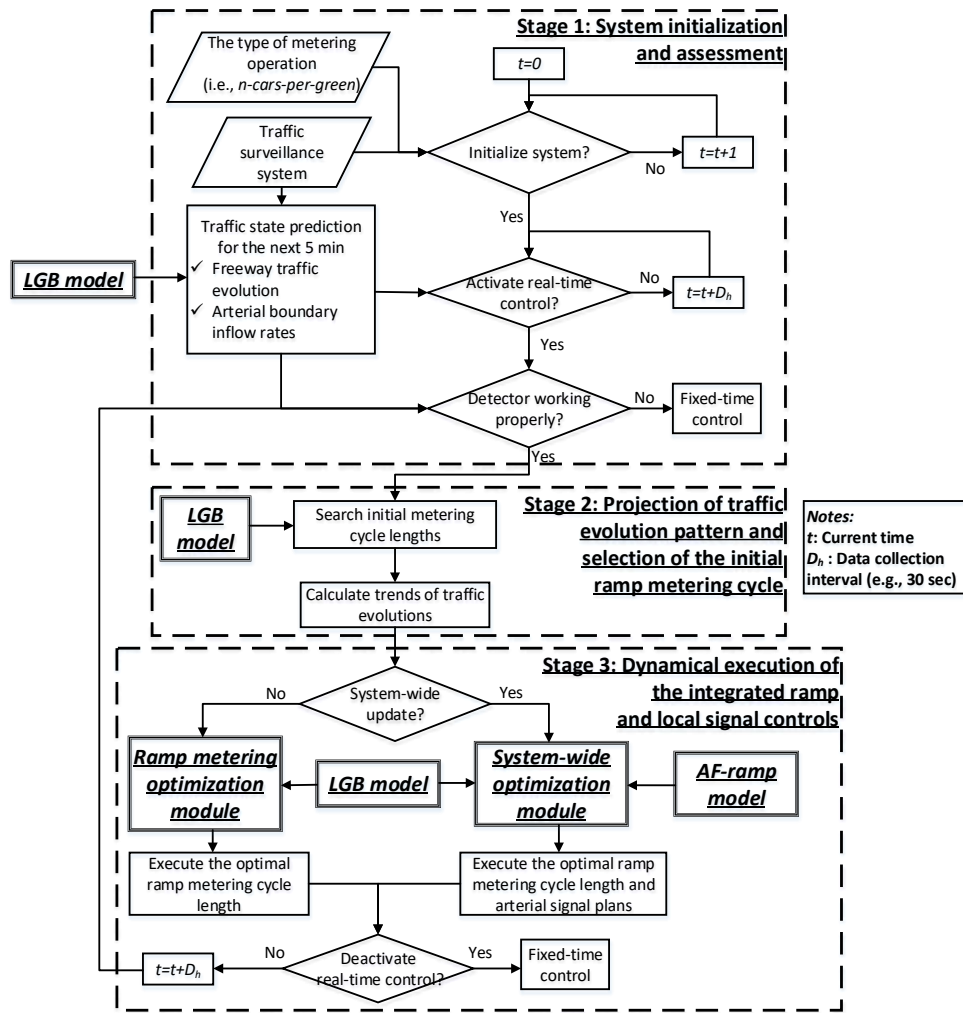


Figure 2.1 The operational flowchart of the proposed RAF-ramp system

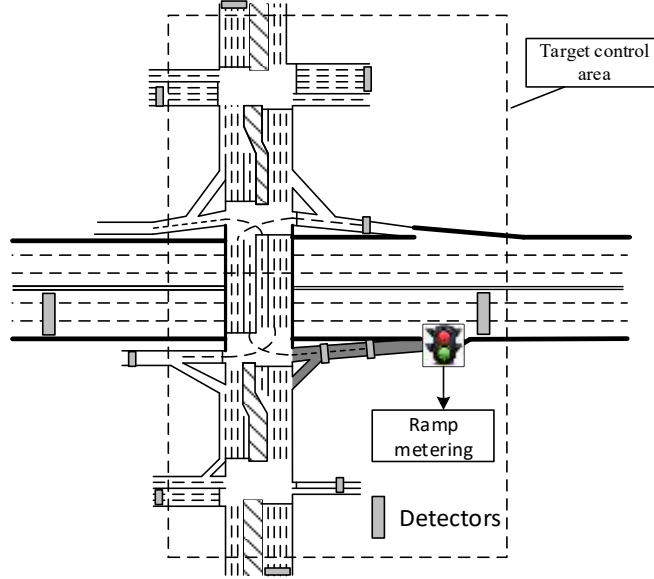


Figure 2.2 Detector locations and the target control area for deploying the RAF-ramp system

Stage 1 – Initialization and assessment

At this stage, the proposed system shall first perform its real-time monitoring of the target area's traffic conditions and then determine when to activate the real-time operations. An essential task to be done concurrently with traffic monitoring is the constant assessment of the detectors' data quality and reliability. Some well-established methods for this task can be found in the literature (Achillides and Bullock, 2004; Lu et al., 2014). The core concepts for system initialization and traffic state monitoring are reported below:

System initialization

Since the LGB module, macroscopic in nature, needs the initial roadway traffic conditions from sensor data to project the traffic state evolution over the selected future time horizon, one can select the time period of 30-60 minutes prior to the peak hours for system initialization, mainly to ensure that its interactions with traffic detectors work as expected and the projected traffic states are consistent with observed conditions.

Traffic state monitoring and prediction

At each current time interval t , the system shall employ the LGB model to predict the flow rates on the freeway segment upstream of the on-ramp over the next N time intervals (i.e., $t+1$ to $t+N$), denoted as $W_t(t+n)$, where $n=1, \dots, N$. Therefore, the expected flow rate on the freeway segment upstream of the on-ramp for a projected time interval k , denoted as $\widehat{W}(k)$, can be calculated with the average of all flow rates predicted from all preceding $(k-N)$ intervals to the current interval t . The mathematical expression of such a process is shown below:

$$\widehat{W}(k) = \frac{W_{k-N}(k) + W_{k-N+1}(k) + \dots + W_t(k)}{N - (k-t) + 1} \quad (2.1)$$

For example, as shown in Figure 2.3, given that the duration of each time interval is 30 sec and with N equal to 10 at the current time of 7:00:00 AM, the system will produce the projected traffic states up to 7:05:00 AM at the time unit of every 30 seconds. Hence, keeping the same prediction exercise, the system with the LGB model up to 7:04:30 am will have ten predicted

traffic flow rates for the interval of 7:05:00 AM, i.e., $W_{7:00:00}(7:05:00)$, $W_{7:00:30}(7:05:00)$, ..., $W_{7:04:30}(7:05:00)$. Then, the system will take the average of those ten predicted results as the expected flow rate for the 7:05:00 AM interval (i.e., $\hat{W}(7:05:00)$). Following the same logic, one can compute the expected flow rates for the following nine time intervals (i.e., 7:05:30 AM to 7:09:30 AM).

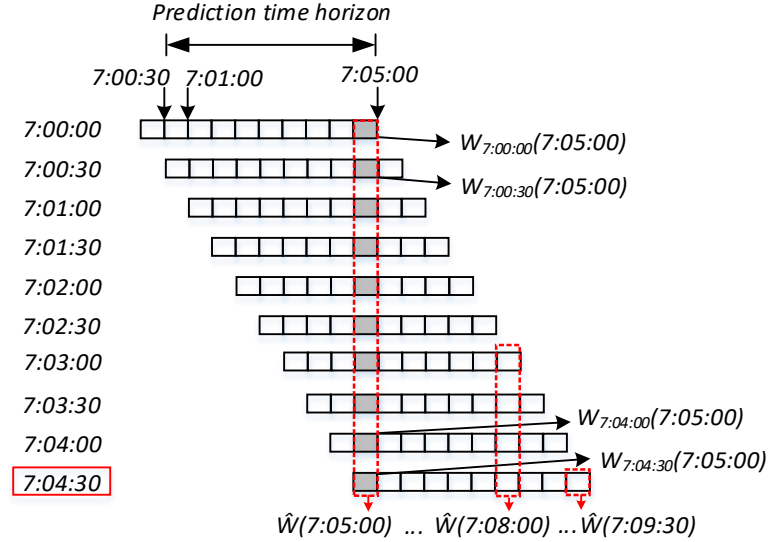


Figure 2.3 Example of calculating expected flow rate for the projected time interval

Given a series of predicted flow rates over the projected time horizon, one can then calibrate the trend for the flow rates, using all obtained $\hat{W}(k)$, where $k = t+1$ to $t+N$, and the slope, a_1 , indicates the evolution trend of $\hat{W}(k)$ over the projected N intervals.

$$f(k) = a_1 \cdot k + b_1 \quad (2.2)$$

Activation mechanism

After initialization, this system will then assess the necessity of activating the real-time control based on the predicted and detected traffic states on the freeway segments upstream of the on-ramp. The main concept is that if at least half of those predicted (detected) flow rates in the subsequent (past) 5 minutes exceed the preset thresholds, then the real-time control ought to be activated. The assessment algorithm is detailed in Table 2.1.

Table 2.1 The Assessment Process for Activating the Real-time Control

Step 1

At time t ,

If (at least half of $\widehat{W}(k)$ in the next 5 min $> \gamma_1$) **and** ($a_1 \geq 0$)

then go to Step 3;

else go to Step 2;

Step 2

If (at least half of the detected flow rates on the freeway segment upstream of the on-ramp over the past 5 min $> \gamma_2$)

then go to Step 3;

else go to Step 4;

Step 3

Stop **and** activate real-time control;

Step 4

$t=t+D_h$ **and** go to step 1.

Note: a_1 presents the slope of the trend line of $\widehat{W}(k)$ in the next 5 min; D_h is the data collection interval (e.g., 30 sec)

Stage 2 – Projection of traffic evolution patterns and selection of the initial ramp metering cycle

The primary task at Stage 2 is to determine the best initial cycle length for ramp metering for the next system-wide control period, occurring every 5 minutes. This is identified using the freeway's flow rates and arterial's signal plans at the current time interval t . More specifically, the system will first employ its LGB model to predict the freeway's throughputs for each time interval over the next 5 minutes. It then applies a search algorithm to identify the corresponding metering cycle that maximizes freeway throughput, provided that discrepancies between projected and actual traffic conditions are within the range of indifference from the control perspective. Such a metering cycle will be subjected to revision every 30 seconds, using the local metering algorithm reported later in Stage 3. The step-by-step description of the control process and search algorithm at this stage is shown in Table 2.2 **Error! Reference source not found.**

Primary information produced during this stage of operations for each projected time interval of 5 minutes includes: 1) the predicted flow rates on the freeway segment upstream of the on-ramp; 2) the predicted arterial boundary inflow rates; 3) the differences between the detected and predicted inflow rates over the arterial's control boundaries; and 4) the detected occupancies at the on-ramp and their evolution patterns.

Table 2.2 Operational Process for the Search of the Optimal Initial Cycle Length for Ramp Metering Control

At the current time t ,

Step 1

Set $t_a = t$ **and** metering cycle length (C_o) = $C_{o,min}$

Step 2

Predict freeway throughput (V_{t_a, C_o}^F) of the period (t_a) to ($t_a + D_h$) with a given metering cycle length, C_o , with the **LGB model**.

Step 3

If $C_o < C_{o,max}$

then $C_o = C_o + 1$ **and** go to Step 2.

else go to Step 4.

Step 4

Choose the metering cycle length with maximal freeway throughput as the preliminary optimal cycle length (\hat{C}_{ta}) for the period (t_a) to ($t_a + D_h$).

Step 5

If $(t_a - t) < 300$ sec

then set $t_a = t_a + D_h$ **and** $C_o = C_{o,min}$ **and** go to Step 2

else stop and output the optimal metering cycle lengths

Note: $C_{o,min}$ is a prespecified lower bound of the metering cycle length; $C_{o,max}$ is a prespecified upper bound of the metering cycle length; and D_h denotes data collection frequency (i.e., 30 sec).

Stage 3 – Dynamical execution of the integrated ramp and local signal controls

System-wide update mechanism

With the information from previous stages, the RAF-ramp system, as shown in Figure 2.4, at this stage will determine whether to execute a system-wide update (i.e., concurrent updates for both the ramp metering cycle length and arterial signal plans) or maintain the dynamic ramp control for the next interval of five minutes.

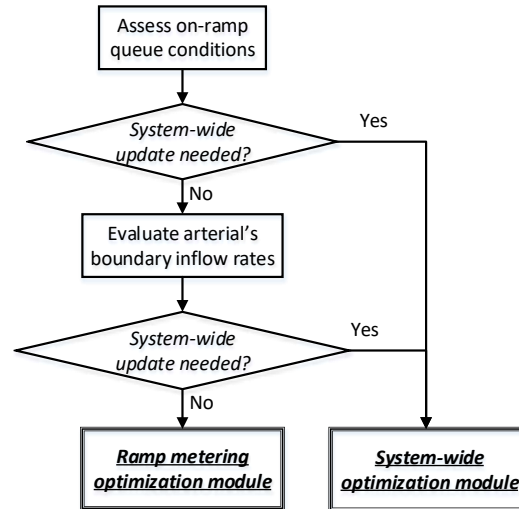


Figure 2.4 Flowchart of the system-wide update mechanism

The core logic for the Stage 3 assessment is to first estimate the on-ramp queues based on the initial metering cycle produced at Stage 2, along with the projected the arterial flow rates moving into the control area. The system then evaluates the need for the system-wide update under the following conditions:

- The initial ramp metering cycle lengths from Stage 2 will cause the on-ramp queue to spill back in the next 5 minutes based on the assessment process shown in Step 1 in Table 2.3, where $\Theta(Q^A)$ is the pre-specified maximum allowable ramp metering cycle under the critical arterial traffic volume, Q^A , that ensures no overflows at the ramp over the next 5 minutes.
- The on-ramp is currently experiencing queue overflows based on the occupancies detected by the on-ramp detectors (see Step 2 in Table 2.3).
- The on-ramp queues are projected to consistently decrease over the next 5 minutes based on the estimation process shown in Step 3 of Table 2.3.

Note that if the differences between the predicted and detected arterial inflow rates to the control area over the past 5 minutes have consistently exceeded the prespecified criteria, it is also a justification for the system to concurrently reoptimize the ramp metering and arterial signal controls.

Table 2.3 Procedure for Assessing the On-ramp's Queue Conditions

Step 1

If (at least half of the initial metering cycles for ramp control over the next 5 min determined in Stage 2 $> \Theta(Q^A)$) **and** ($S(\text{predicted flow rates on the freeway segment upstream of the on-ramp}) \geq 0$) **and** ($S(\text{predicted local boundary inflow rates}) \geq 0$)

then go to Step 4;

else go to Step 2;

Step 2

If ($S(\text{predicted arterial boundary inflow rates}) \geq 0$) **and** ($S(\text{detected occupancy rates of the upstream detector of the on-ramp}) \geq 0$) **and** ($\sigma_u^O(t - n_1 \cdot D_h) \geq 25\%$, $n_1 = 0 \text{ and } 1$) **and** ($\sigma_m^O(t - n_2 \cdot D_h) \geq 25\%$, $n_2 = 0, 1, \dots, 5$)

then go to Step 4;

else go to Step 3;

Step 3

If ($S(\text{detected occupancy rates at the middle detector on the on-ramp}) < 0$) **and** ($S(\text{predicted arterial boundary inflow rate}) \leq 0$)

then go to Step 4;

else go to Step 5;

Step 4

Stop **and** output "system-wide update needed."

Step 5

Stop **and** output "system-wide update not needed."

Note: $\sigma_u^O(t)$ and $\sigma_m^O(t)$ denote the occupancy rates of the upstream and middle detectors on the on-ramp at time t , respectively; an occupancy threshold of 25% is used to determine whether the queue has reached the VDs or not (Liu et al., 2007); and D_h is the data collection frequency (e.g., 30 sec).

Real-time deactivation mechanism

Table 2.4 shows both the criteria and procedures for assessing if the system should deactivate its real-time operations and stay at the pre-timed or time-of-day mode. The core criteria for justifying such deactivations are as follows: 1) the computed ramp metering cycle lengths are consistently equal to the predefined minimum value; 2) the occupancies detected by the on-ramp detector are consistently lower than a prespecified threshold; 3) the detected arterial boundary inflow rates are consistently less than a predefined threshold; and 4) the detected arterial boundary inflow rates exhibit a non-increasing trend.

Table 2.4 Procedure for Deactivation of Real-time Control

Step 1

At time t , for the past 10 min,

If (the computed ramp metering cycle lengths $=C_{o,min}$) **and** ($\sigma_u^O(k') < \gamma_5$) **and** (detected arterial boundary inflow rates $< \gamma_6$) **and** ($S(\text{detected arterial boundary inflow rates}) \leq 0$)

then go to Step 2;

else go to Step 3;

Step 2

Stop **and** deactivate real-time control

Step 3

Stop **and** continue real-time control

Note: $C_{o,min}$ is a prespecified lower bound of the metering cycle length; $\sigma_u^O(k')$ denote the occupancy rates of the upstream detectors on the on-ramp at time k' ; $S(.)$ presents the slope of the trend line of the target variable; and γ_5 and γ_6 are predefined thresholds.

2.3 System optimization module

The system-wide optimization module, which integrates the LGB (Chen et al., 2021) and AF-ramp (I) models, functions to maximize the total benefit of all motorists on the freeway segments and its neighboring arterial segments based on real-time detected traffic conditions. The module is embedded with the following sets of constraints: 1) freeway throughput constraints to reflect its relation with the ramp metering cycle; 2) time-dependent on-ramp constraints to prevent on-ramp overflows; 3) intersection queue constraints for minimizing intersection queue spillovers; and 4) intersection flow conservation and signal timing related constraints. The flowchart of the system-wide optimization module is shown in Figure 2.5.

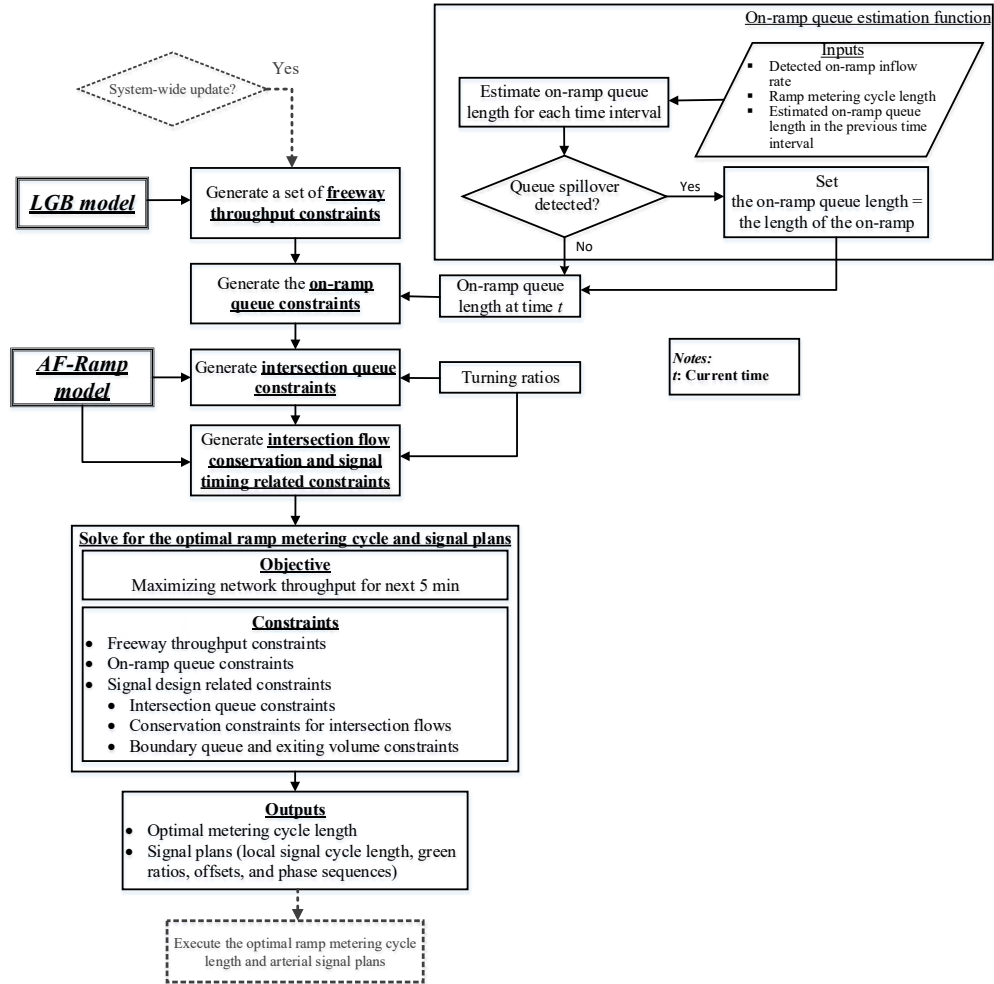


Figure 2.5 The flowchart of the system-wide optimization module

Note that the proposed system-wide optimization module is developed with the core concept of the AF-ramp model and some essential enhancements to ensure the effectiveness of its real-time operation. Specifically, the AF-ramp model is designed to maximize the total throughput at both the freeway on-ramp segment and the boundary links within the neighboring local arterial while ensuring no on-ramp queue spillback and progression for multi-path flows on the arterial links based on the historical traffic volume data. To advance the AF-ramp model from a time-of-day off-line model to real-time operations, the proposed system has been incorporated with the following enhancements: 1) utilizing the LGB model for real-time estimation of freeway capacity; and 2) establishing the time-dependent on-ramp queue constraints. Those formulations along with key constraints from the AR-ramp model are introduced with the key notations listed in Table 2.5.

Table 2.5 Key Notations Used in the System-wide Optimization Module

Sets	
Ω	Set of intersection movements heading to the on-ramp
Δ	Set of movements exiting the target network
Φ	Set of movements entering the target network
$D_{I,J}$	The set of lane groups in the adjacent <i>downstream</i> segment connected to lane group J in segment I ($ D_{I,J} $ is the number of lane groups in $D_{I,J}$)
$S_{I,J}$	The set of lane groups in the adjacent <i>upstream</i> segment connected to lane group J in segment I ($ S_{I,J} $ is the number of lane groups in $S_{I,J}$)
Parameters	
L_o	On-ramp length (veh)
$s(s_o)$	Saturation flow rate at intersections (the ramp metering point) (veh/hr)
t_i	Travel time from intersection i to $i+1$ (in cycle);
$V_{\mu,i}$	Volume demand for movement μ at intersection i (veh/hr)
$f_{\mu,i}$	Lane use factor based on the number of lanes for movement μ at intersection i
$r_{\mu,i}$	Volume ratio of movement μ from arterial at intersection i
$L_{b,i}, L_{l,i}$	Bay length and the link length at intersection i (veh)
t_l	Lost time for each signal phase(sec)
T_t	Time duration of the study (hr)
γ	Robustness factor that represents the sensitivity of volume fluctuation to the occurrence of queue spillback
\dot{n}	Number of vehicles that are permitted to pass the ramp meter per each green interval
L_I	Length of freeway segment I
H	Average vehicle length (ft)
T	Time interval for updating the traffic state
Z	Number of total time intervals
K	Number of elapsed time intervals
v^m	Minimum speed of freeway vehicles
$\lambda_{I,J}$	Number of lanes in lane group J in segment I
ρ^{jam}	Freeway jam density
ρ_I^C	Critical density of segment I
β_1, β_2	Weighting factors in the objective function
$\eta, \tau, \nu, \kappa, \phi$	Parameters in the LGB model
Variables for local arterial	
R_i	Number of queuing vehicles outside the target area due to the limited green time (veh/hr)
$l_p(\dot{k})$	Queue length caused by excessive demand at time \dot{k} (veh)
l_e	Queue length caused by arrivals from the upstream intersection in every cycle (veh)
ξ	Reciprocal of the cycle length at the arterial intersections (/sec)

$b_{m,i}$	Local progression bands, i.e., the duration within which vehicles from traffic path m can traverse intersections $i-1$ and i without stop (in cycle)
$t_{\mu,i}^a, t_{\mu,i}^b$	Start and end of the green phase for downstream movement μ at intersection i
$\tau_{d(m),i}$	Queue clearance time of movement $d(m)$ at intersection i (in cycle)
$l_{\mu,i}$	Queue length for movement μ at intersection i (veh)
V^A	Arterial throughput at the boundary outbound links (veh/hr)
V_{μ}^a	Actual Volume for movement μ at intersection i (veh/hr)
Δk	Duration of one time interval for the local arterial variable updates

Variables for LGB model

$\alpha_{J,J+1}$	Target density ratio between lane groups J and $J+1$
C_o	The metering cycle length (sec)
$C_{o,min}/C_{o,max}$	The minimal/maximal metering cycle length (sec)
$N_{I,J,J+1}(k)$	Number of vehicles changing from lane group J to $J+1$ in segment I at time k . ($J = I, \dots, G_I - 1$; G_I is the number of lane groups in segment I)
$q_{I,J}(k)$	Flow rate of lane group J in segment I at time k (veh/hr)
$q_o(k)$	Outflow rate of the on-ramp at time k (veh/hr);
$\hat{q}_o(k)$	Inflow rate of the on-ramp at time k (veh/hr);
$S_a(k)$	Remaining space in the acceleration lane at time k (veh)
$V_I(\cdot)$	Speed-density relation for segment I
V^F	Freeway throughput at the downstream of the on-ramp segment (veh/hr)
\hat{V}_{ω}	Freeway throughput under the given metering cycle, ω , obtained by adding up the throughputs of all lanes of the segment downstream of the on-ramp
$v_{I,J}(k)$	Speed of lane group J in segment I at time k (kph)
$w_o(k)$	Number of vehicles in the on-ramp queue at time k
$\rho_{I,J}(k)$	Density of lane group J in segment I at time k (prior to receiving lane-changing vehicles)
$\rho_{I,J}^*(k)$	Density of lane group J of segment I at time k (after accommodating lane-changing vehicles)

Freeway throughput constraints

The first set of constraints have been constructed to reflect the relationship between the given ramp cycle length, ω , and the resulting freeway throughput, denoted as \hat{V}_{ω} . Note that one constraint will be generated for each possible value of C_o so that the system-wide optimization module can precisely select the ramp metering cycle length that yields the highest total throughput for both the freeway segment and the local arterial.

$$V^F = \hat{V}_{\omega}, \text{ if } C_o = \omega (\forall \omega \in [C_{o,min}, C_{o,max}]) \quad (2.3)$$

where, \hat{V}_{ω} is the freeway throughput under the given metering cycle, ω , obtained by adding up the throughputs of all lanes of the segment downstream of the on-ramp, $q_{I,J}(k)$, which can be explicitly predicted with the LGB model. By integrating the LGB model, nonconvex in nature, to

the optimization formulation, one can effectively capture the complex traffic dynamics and also yield the solution sufficiently efficient for real-time needs.

$$\hat{V}_\omega = \sum_{k=t+1}^{t+N} \sum_{I,J} q_{I,J}(k) \quad (2.4)$$

The key formulations of the LGB model to yield the $q_{I,J}(k)$ under each possible value of metering cycle length are summarized below. A more detailed description of the model can be found elsewhere (Chen et al., 2021).

The number of lane-changing vehicles

$$N_{I,J,J+1}(k) = \begin{cases} \min(L_I \rho_{I,J}(k), \eta \lambda_{I+1,J} \lambda_{I+1,J+1} L_{I+1} \frac{\rho_{I+1,J}(k) - \rho_{I+1,J+1}(k)}{\lambda_{I+1,J} + \lambda_{I+1,J+1}}), & (\rho^{jam} - \rho_{I,J+1}(k)) L_I, \text{ if } \rho_{I+1,J}(k) > \rho_{I+1,J+1}(k) \\ 0, & \text{otherwise} \end{cases} \quad (2.5)$$

$$N_{I,J,J+1}(k) = \begin{cases} \min(\lambda_{I,J} \lambda_{I,J+1} L_i \frac{\rho_{I,J}(k) - \alpha_{J,J+1} \rho_{I,J+1}(k)}{\lambda_{I,J} \alpha_{J,J+1} + \lambda_{I,J+1}}, & (\rho^{jam} - \rho_{I,J+1}(k)) L_I, \text{ if } \rho_{I,J}(k) > \alpha_{J,J+1} \rho_{I,J+1}(k) \\ 0, & \text{otherwise} \end{cases} \quad (2.6)$$

Flow rate and density calculation

$$\rho_{I,J}(k+1) = \begin{cases} \rho_{I,J}^*(k) + \frac{T}{L_I \lambda_{I,J}} \left[\frac{\lambda_{I,J}}{\lambda_{I-1,J}} q_{I-1,J}(k) - q_{I,J}(k) \right], & \text{if } \lambda_{I,J} \leq \lambda_{I-1,J} \\ \rho_{I,J}^*(k) + \frac{T}{L_I \lambda_{I,J}} \left[\left[\sum_{m \in S_{I,J}} \lambda_{I-1,m} q_{I-1,m}(k) \right] - q_{I,J}(k) \right], & \text{if } \lambda_{I,J} > \lambda_{I-1,J} \end{cases} \quad (2.7)$$

$$q_{I,J}(k) = \lambda_{I,J} \rho_{I,J}^*(k) v_{I,J}(k) \quad (2.8)$$

$$\rho_{I,J}^*(k) = \rho_{I,J}(k) + \frac{N_{I,J-1,J}(k) - N_{I,J,J+1}(k)}{L_I \lambda_{I,J}} \quad (2.9)$$

$$q_o(k) = \min \left\{ (\hat{q}_o(k) + \frac{w_o(k)}{T/3600}), \frac{2 * \dot{n} * S_o}{\omega}, \frac{S_a(k)}{T/3600} \right\} \quad (2.10)$$

Speed update

$$v_{I,J}(k+1) = \max \{ v^m, v_{I,J}(k) + \frac{T}{\tau} [V_I(\rho_{I,J}^*(k)) - v_{I,J}(k)] + \frac{T}{L_I} v_{I,J}(k) \left[\frac{\sum_{m \in S_{I,J}} (v_{I-1,m}(k))}{|S_{I,J}|} - v_{I,J}(k) \right] - \frac{vT}{\tau L_I} \frac{\sum_{w \in D_{I,J}} (\rho_{I+1,w}^*(k))}{|D_{I,J}|} - \rho_{I,J}^*(k) \right] - \frac{\phi \max(v_{I,J}(k) - v_{I,J-1}(k), 0) N_{I,J-1,J}(k)}{L_I \lambda_{I,J} \rho_I^c} \} \quad (2.11)$$

Equations 2.5 and 2.6 are developed to calculate the number of lane-changing vehicles between lane groups within the on-ramp segments and the downstream segments, respectively. Equation 2.7 formulates the dynamics of density evolution for each lane group using the flow conservation relation, which utilizes the lane group density after receiving the lane changing vehicles ($\rho_{I,J}^*(k)$) and flow rate ($q_{I,J}(k)$) specified in Equations 2.8 and 2.9. The on-ramp outflow

rate is determined by Equation 2.10. In addition, Equation 2.11 is specified to reflect the speed dynamics for each lane group within each segment.

Note that a new set of Equation 2.3 should be produced, based on the output of the LGB model once the system-wide optimization is required to reflect the real-time relation between freeway throughput and the ramp metering cycle to be applied.

On-ramp queue constraints

The on-ramp queue constraints are developed to ensure that the on-ramp queue under ramp metering control would not exceed the ramp's length during the entire control period. Conceivably, the ramp queue consists of residual queues due to the difference between the on-ramp's entering and exiting flow rates and the arriving vehicles discharged from those intersections within the control zone per cycle. One can formulate Equation 2.12 to calculate the former at the end of the next control interval and let the latter be expressed by Equation 2.13.

$$l_p(\dot{k} + 1) = \max (w_o(\dot{k}) + (\sum_{\mu \in \Omega} V_\mu^a - s_o r_o) \cdot \frac{\Delta k}{3600}, 0) \quad (2.12)$$

$$l_e(\dot{k} + 1) = \sum_{\mu \in \Omega} V_\mu^a / 3600 \xi \quad (2.13)$$

$$w_o(\dot{k}) = \max (\min (w_o(\dot{k} - 1) + \frac{\Delta k}{3600} * (\hat{q}_o(\dot{k} - 1) - q_o(\dot{k} - 1)), \frac{L_o}{H}), 0) \quad (2.14)$$

where $l_p(\dot{k} + 1)$, denoting the on-ramp queue length due to excessive on-ramp flows at the end of time interval $(\dot{k} + 1)$, is to be updated by the on-ramp queue estimation function when no queue spillover is detected by the on-ramp detector, as shown in Equation 2.14. If a queue spillover is detected, $w_o(\dot{k})$ will be set to (L_o/H) . Note that such queue length $l_p(\dot{k} + 1)$ may decrease during the next control interval if the on-ramp arriving flow rate is lower than the metering rate. The right-hand side of Equation 2.13 is to sum up all traffic flows entering the on-ramp during one signal cycle from the intersections.

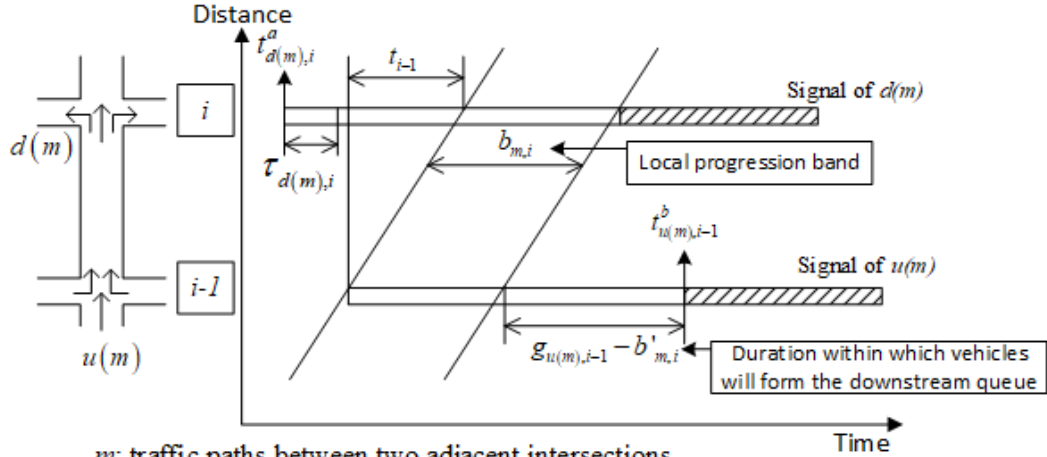
To ensure that the on-ramp queue length would not increase rapidly at the start of the peak period, the allowed upper bound for the on-ramp queue length should be time-dependent, based on the ratio of the elapsed time over the total period, as expressed in Equation 2.15.

$$l_p(\dot{k}) \leq \min ((\frac{k}{z}(L_o/H - l_e(\dot{k})), (L_o/H - l_e(\dot{k}))) \quad (2.15)$$

In Equation 2.15, $(L_o/H - l_e(\dot{k}))$ is to calculate the available space for the vehicle queues caused by excessive on-ramp flows.

Intersection queue constraints

To ensure that the proposed ramp control will not cause queue spillback at those intersections feeding flows to the freeway, the proposed system adopts the formulations in the AF-ramp model to estimate the number of vehicles stopping at the intersections within the ramp's impacted area. Figure 2.6 illustrates the local progression band for one traffic path on an arterial link, where the specially designed signal plan, coordinated with ramp control, can ensure that the intersection queues will not overflow from their designated links.



m : traffic paths between two adjacent intersections

$u(m) \in \{\text{through, left-turn from side street, right-turn from side street}\}$

$d(m) \in \{\text{through, left-turn, right-turn}\}$

Figure 2.6 Local paths between two adjacent intersections near the on-ramp

The intersection queue constraints can be summarized as below:

$$b_{m,i} = \min\left(t_{d(m),i}^b, t_{u(m),i-1}^b + t_{i-1}\right) - \max\left(t_{d(m),i}^a + \tau_{d(m),i}, t_{u(m),i-1}^a + t_{i-1}\right) \quad (2.16)$$

$$l_{\mu,i} = \sum_{d(m)=\mu} V_{u(m),i-1}^a r_{d(m),i} \left(g_{u(m),i-1} - b_{m,i-1}\right) f_{d(m),i} / 3600\xi, \mu=\text{through or left-turn} \quad (2.17)$$

$$l_{\mu,i} \frac{s}{s - V_{\mu,i} f_{\mu,i}} \times \gamma \leq L_{b,i} \quad (2.18)$$

$$l_{\mu,i} \frac{s}{s - V_{\mu,i} f_{\mu,i}} \times \gamma \leq L_{l,i} \quad (2.19)$$

$$\tau_{\mu,i} = l_{\mu,i} \frac{3600\xi}{s - V_{\mu,i} f_{\mu,i}} \quad (2.20)$$

where, Equation 2.16 is for calculating the local band between two intersections for traffic stream m , i.e., a period during which vehicles would pass two adjacent intersections without encountering red phases; Equation 2.17 calculates queue lengths on the left-turn lanes and through lanes of the arterial links based on the local bandwidths; Equations 2.18 and 2.19 ensure that the maximum queue length during a cycle would not exceed the turning bay or the link length; and Equation 2.20 is for estimating the queue discharging time. Note that the traffic volume in the above equations is updated in real-time based on the traffic detected at the boundary links of the network.

The remaining essential yet fundamental formulations, including intersection flow conservation equation and green time allocation constraints, are identical to those in the AF-ramp model (Cheng and Chang, 2021).

Objective function for system control

Note that the system-wide optimization module is focused on maximizing the total throughput for the freeway and the local arterial. Furthermore, those queueing vehicles that may not be able to enter the control area due to the shorter cycle length and green ratio shall result in a penalty to the objective function since these vehicles would incur excessive delay if not properly discharged. Therefore, the objective function of the system-wide control model can be expressed as below,

$$\begin{aligned} & \text{Max } V^F + \beta_1 V^A - \beta_2 \sum_{i \in \omega} R_i \\ & \text{s.t.} \end{aligned}$$

Freeway throughput constraint: Equation 2.3

On-ramp queue constraints: Equations 2.12-2.15

Intersection queue constraints: Equations 2.16-2.20

Intersection flow conservation and signal timing related constraints (Cheng and Chang, 2021)

With the above objective function and constraints, the optimization model can be formulated into Mixed Integer Linear Programming (MILP), and thus can be solved by various commercial packages.

2.4 Ramp metering optimization module

The flowchart of the ramp metering optimization module for the proposed system is shown in Figure 2.7. When reoptimizing the ramp control alone is justified at Stage 3 of the operations, its primary control objective is to maximize the freeway throughput. Following the logic of the system-wide optimization module, the LGB model will be adopted to predict the freeway throughputs under the set of candidate metering cycle lengths (i.e., between maximal and minimal metering cycle lengths), as expressed with the right-hand side terms of Equation 2.3. The complete ramp metering optimization module is shown below,

$$\begin{aligned} & \text{Max } V^F \\ & \text{s.t.} \end{aligned}$$

Freeway throughput constraint: Equation 2.3

Where, V^F is the freeway throughput.

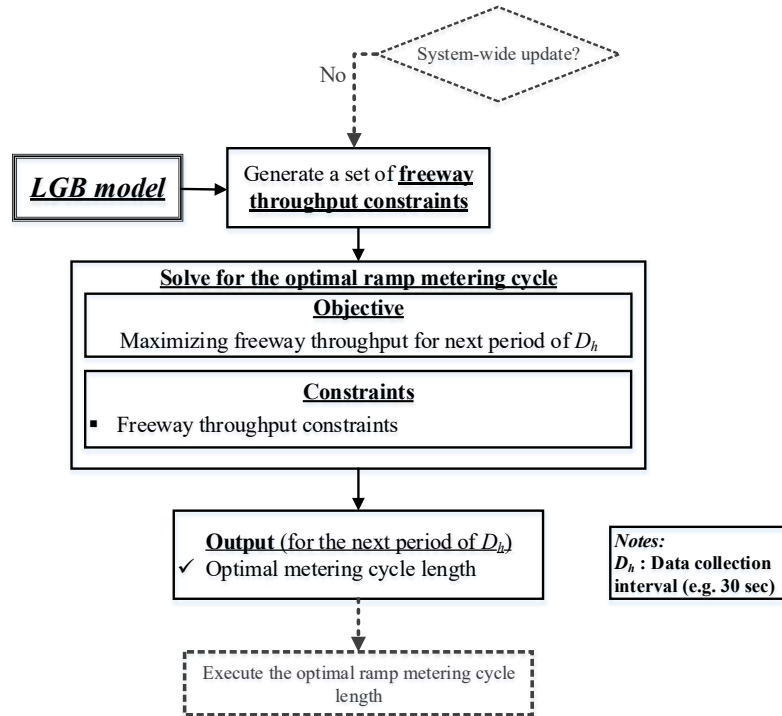


Figure 2.7 The flowchart of the ramp metering optimization module

2.5 Numerical evaluations

The case study is designed to demonstrate the effectiveness of the proposed RAF-ramp system on 1) smoothing the freeway traffic conditions; 2) preventing overflows at the on-ramp and local arterial's turning bays; and 3) maximizing the total throughput as well as minimizing the total delay for the control area. The proposed system will also be compared with a widely-applied real-time ramp metering model, ALINEA/Q (Smaragdis and Papageorgiou, 2003), and the AF-ramp model (Cheng and Chang, 2021), which is the pre-timed version of the proposed system, with respect to multiple measures of effectiveness (MOEs), including average speeds, maximal on-ramp and intersection queue lengths, and total throughputs as well as delays.

Test site and experimental design

The freeway mainline merging segment at Exit 36 of I-495 Inner Loop in Maryland, U.S., and its neighboring local intersections are adopted as the study site. Figure 2.8 illustrates the test site's geometric features and the locations of its vehicle detectors (VD). The average flow rates and the intersection turning ratios of three experimental scenarios are shown in Table 2.6 and Table 2.7, respectively. To evaluate the robustness of the proposed system's performance, the freeway's mainline flow rates in Scenarios 2 and 3 are set to be 5 percent higher and 5 percent lower than those of Scenario 1, respectively. The phasing plans for all neighboring local intersections are prespecified and shown in Table 2.8, but their green splits, as well as phase sequences, are to be optimized with the proposed system. In addition, the green splits, phase sequences, and metering rates of the fixed-time plan optimized with the average flow rates between 600 to 3000 sec in scenario 1 are shown in Table 2.9.

Note that the metering control in the case study is operated with the practice of 2-cars per green interval. The time interval of 30 seconds is adopted for updating the ramp metering cycle and 5 minutes for the system-wide optimization that includes local signal plans and offsets.

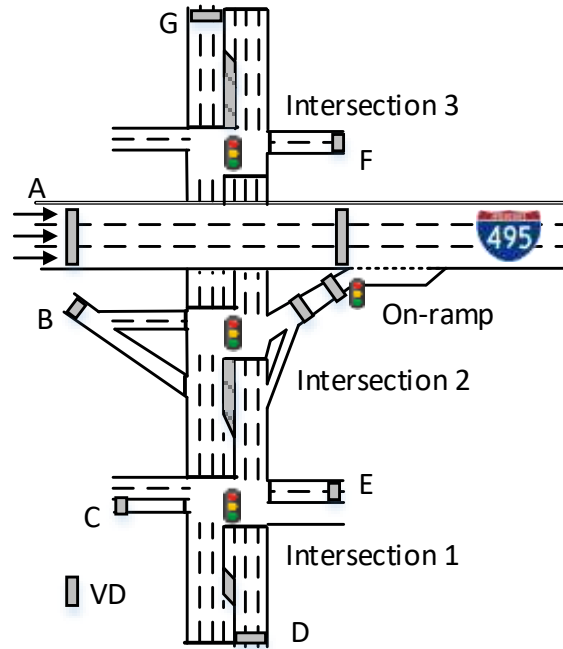


Figure 2.8 The test site's geometric features and locations of its detectors

Table 2.6 Time-varying Flow Rates under Three Experimental Scenarios Unit: vph

Time (sec.)	Scenario	A (3 lanes)	B (1 lane)	C (1 lane)	D (3 lanes)	E (2 lanes)	F (2 lanes)	G (3 lanes)
0 - 600	1	3000						
	2	3150	500	400	1000	800	250	800
	3	2850						
600 - 1500	1	5000						
	2	5250	500	400	1800	800	250	1200
	3	4750						
1500 - 2400	1	4200						
	2	4410	500	400	1200	800	250	1200
	3	3990						
2400 - 3000	1	5000						
	2	5250	500	400	1800	800	250	1200
	3	4750						
3000 - 3600	1	3500						
	2	3675	500	400	1000	800	250	800
	3	3325						

Table 2.7 Intersection Turning Ratios under Three Experimental Scenarios

Intersection	NB			SB			EB			WB		
	L	T	R	L	T	R	L	T	R	L	T	R
1	0.01	0.98	0.01	0.04	0.95	0.01	0.92	0.04	0.04	0.39	0.01	0.6
2	-	0.8	0.2	0.25	0.75	-	0.2	0	0.8	-	-	-
3	0.14	0.86	-	-	0.8	0.2	-	-	-	0.5	0	0.5

Table 2.8 Phase Plans for Three Intersections within the Control Area

Phase ID Intersection	Phase ID			
	1	2	3	4
1				
2				
3				

Table 2.9 Singal Plans for Three Intersections within the Control Area

Phase Intersection	Phase				
	1	2	3	4	Offset
1	19s 	48s 	30s 	23s 	0
2	26s 	54s 	40s 		0
3	30s 	61s 	29s 		0

Cycle Length: 120s

Metering rate: 0.33 (The metering control in the case study will be under 2-cars-per-green operation)

Design of the simulator for real-time simulation analysis

Figure 2.9 shows the simulator used to evaluate the proposed control system under real-time operations. Its traffic simulation module is built with VISSIM 10 (PTV, 2018), and the control

module, including the LGB model, is coded with VB.NET to reflect its interactions with simulated traffic conditions via the VISSIM's COM interface. All vehicle detectors, needed for real-time control and system evaluation, are shown in Figure 2.8. All such detected traffic information, as shown in Figure 2.9, will be transmitted to the RAF-ramp system's simulator constantly through the COM interface to predict traffic states and optimize control strategies for the projected time horizon.

The optimization modules are solved with Gurobi 9 (Gurobi Optimization, 2020) on a Windows 10 desktop with an Intel Core i7-9700 processor and 16 GB RAM. The computation times for system-wide optimization and the optimization of ramp metering update models are less than 10 seconds and 1 second, respectively. The resulting MOEs for performance comparison, are measured directly from the simulator's output.

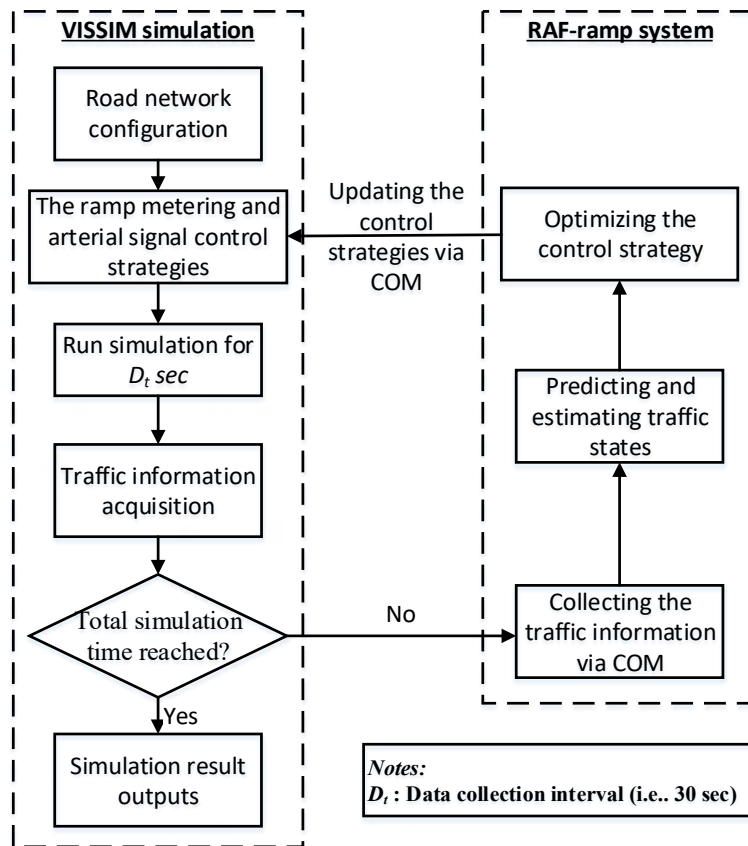


Figure 2.9 The structure of the simulator for simulating real-time operations of the RAF-ramp control system

Performance under the medium-volume scenario (Scenario 1)

Figure 2.10, Figure 2.11, and Figure 2.12 show the average lane speeds on the freeway's merging segment under the control of the RAF-ramp system, ALINEA/Q, and AF-ramp system, respectively, under Scenario 1. Since the traffic on the outermost lane of the freeway merging area is affected by the merging flow most, Figure 2.13 shows the comparisons of the average speeds on the outermost lane (i.e., lane 1) under Scenario 1 with all three control strategies. Figure 2.14 shows the resulting distributions of queue lengths associated with each intersection approach under this scenario.

As shown in Figure 2.10, the lane speeds under the proposed RAF-ramp system are constantly above 40 kph (km per hour). However, this traffic scenario frequently triggers the queue override function in ALINEA/Q and causes the freeway mainline traffic to break down. For example, speeds on the outermost lane are mostly below 40 kph during periods when the queue override function is executed, as shown in Figure 2.11. The performance results from this experimental scenario seem to confirm the benefits of having optimal coordination between the on-ramp metering and its neighboring intersections. It is noticeable that the queues on all links under RAF-ramp, ALINEA/Q, and AF-ramp controls do not spill back to neighboring intersections under this scenario (see Figure 2.14).

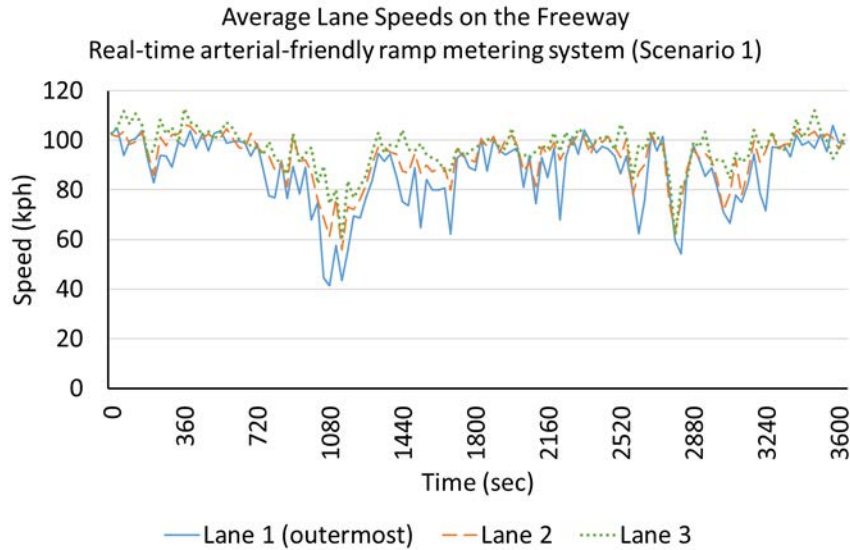


Figure 2.10 Average lane speeds on the freeway's merging segment under the RAF-ramp control

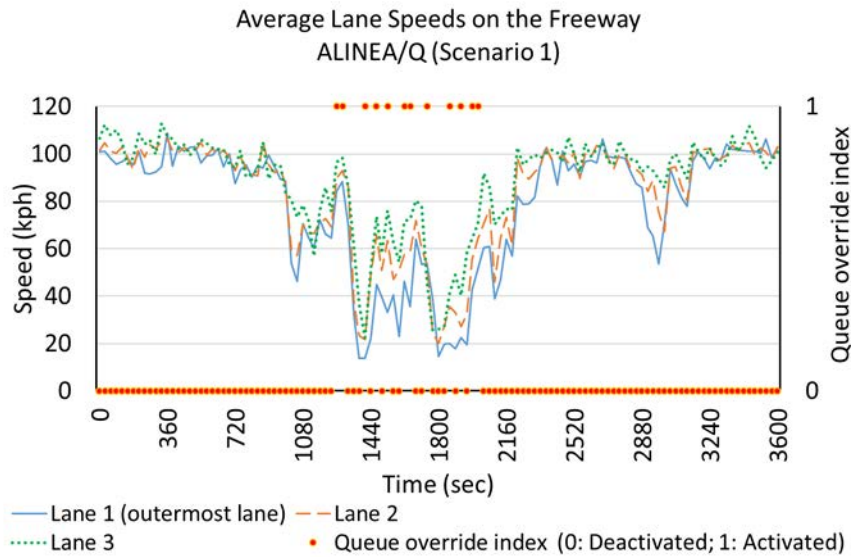


Figure 2.11 Average lane speeds on the freeway's merging segment under ALINEA/Q control

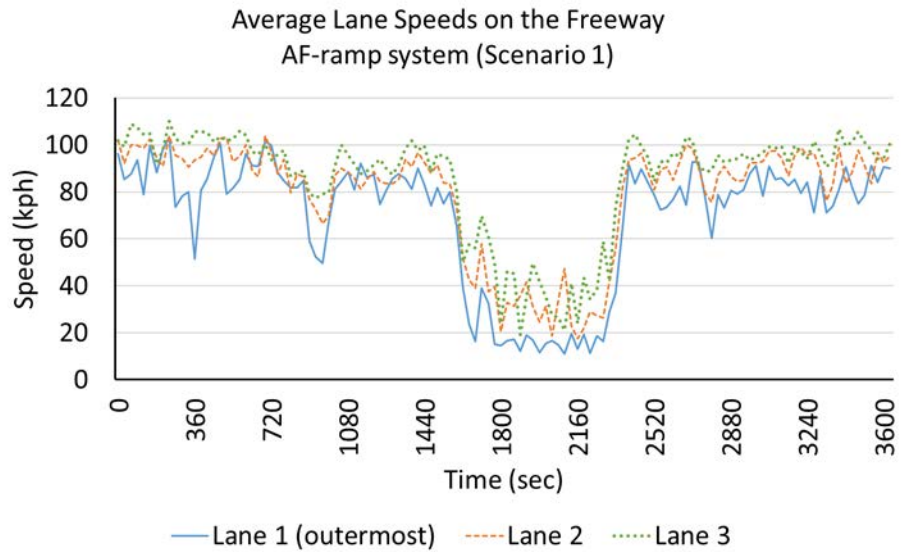


Figure 2.12 Average lane speeds on the freeway's merging segment under the AF-ramp system

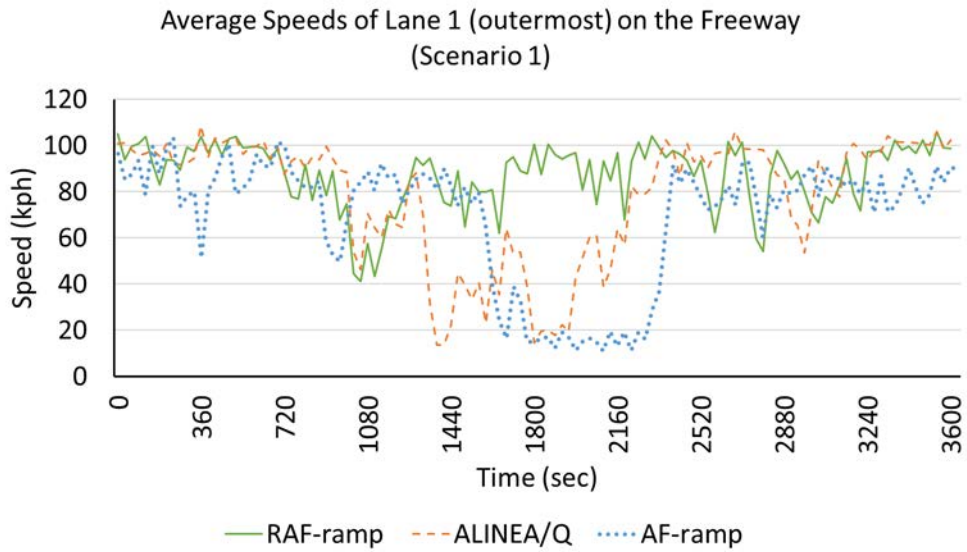


Figure 2.13 Comparison of average speeds of lane 1 (outermost) on the freeway's merging segment

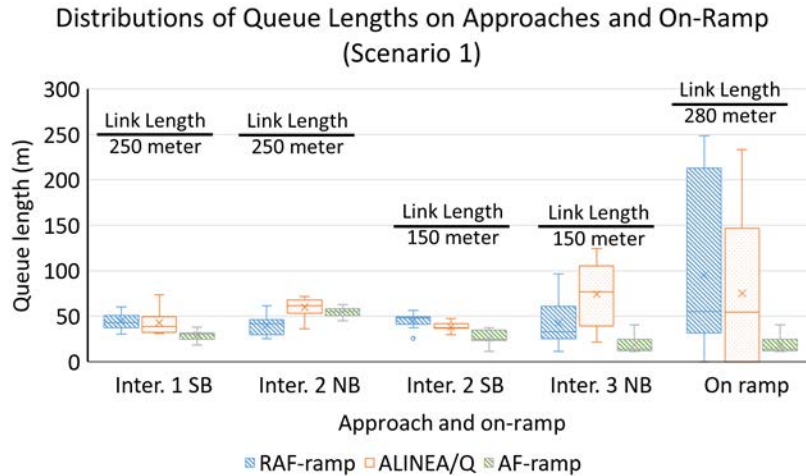


Figure 2.14 Distributions of queue lengths at different intersection approaches

Performance under the high-volume experimental scenario (Scenario 2)

Figures 2.15-2.19, respectively, show the freeway's lane speeds and the distributions of queue lengths with the RAF-ramp, ALINEA/Q, and AF-ramp controls under Scenario 2. The average lane speeds on the target freeway segment with the proposed system remain above 40 kph (see Figure 2.15) under a high-volume traffic condition. In contrast, the speeds on the freeway's outermost lane drop below 30 kph during the period when the ALINEA/Q control inevitably executes its queue override function (see Figure 2.16). In addition, the pre-timed control cannot prevent a speed drop, as shown in Figure 2.17. Figure 2.18 presents the comparison among lane 1's speeds under the three control strategies. Furthermore, the total throughput from the control area under the RAF-ramp system in Scenario 2 is 5.34% (6031 vehs vs. 5725 vehs) higher than that with ALINEA/Q.

In brief, the performance results under Scenario 2 further support the benefits of integrating on-ramp metering with local signal controls as modeled in the RAF-ramp system. Such benefits over ALINEA/Q control with ramp-metering are likely to be more pronounced only in higher volume scenarios, as reflected in the differences between MOEs in scenarios 1 and scenario 2. Note that all arterial links, as with scenario 1, do not experience any queue spillback during the entire experimental period under both controls (see Figure 2.19).

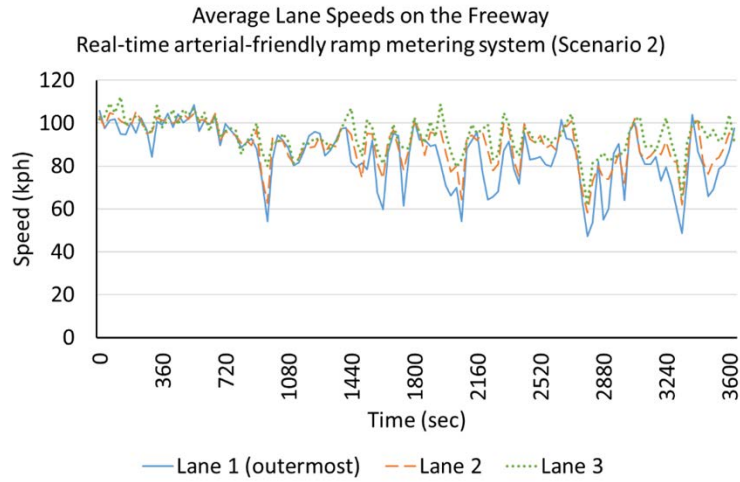


Figure 2.15 Average lane speeds on the freeway's merging segment under RAM-ramp control

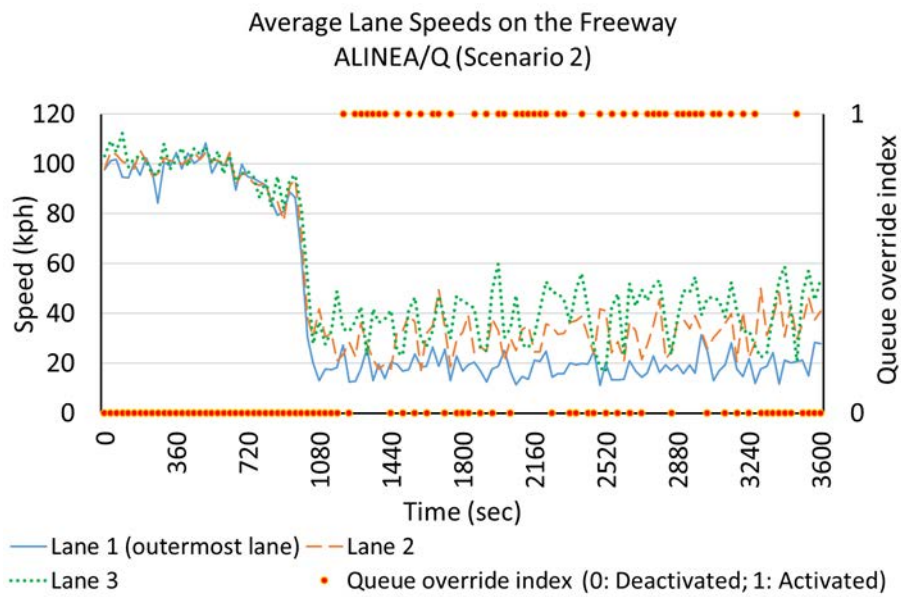


Figure 2.16 Average lane speeds on the freeway's merging segment under the ALINEA/Q control

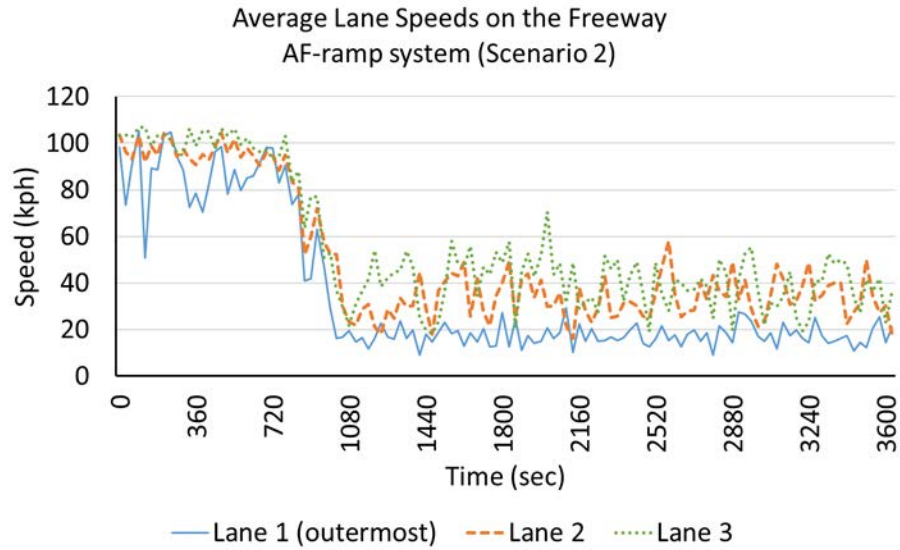


Figure 2.17 Average lane speeds on the freeway's merging segment under the AF-ramp system

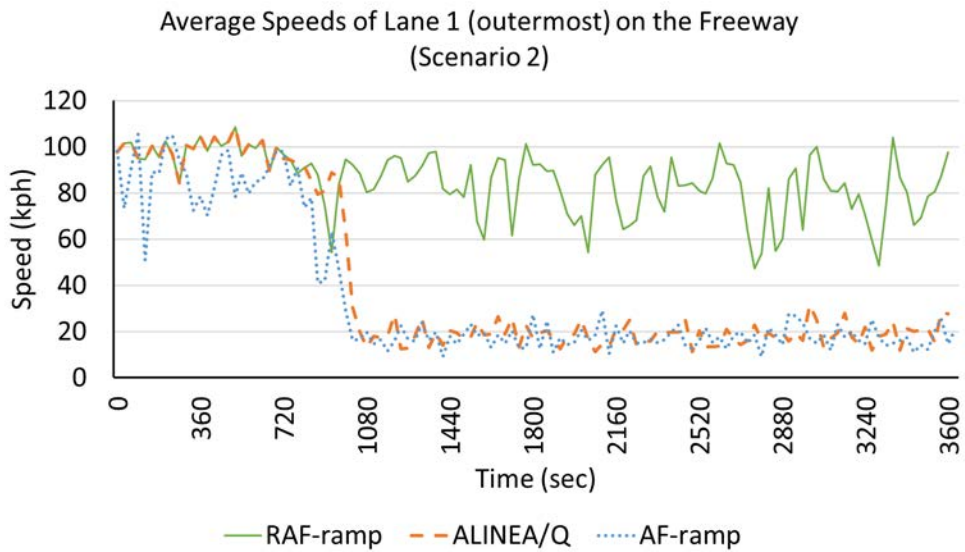


Figure 2.18 Comparison of average speeds of lane 1 (outermost) on the freeway's merging segment

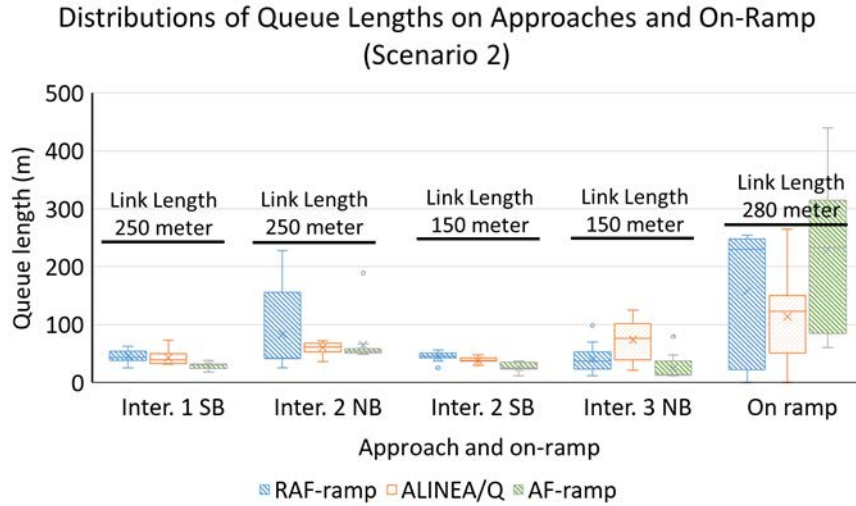


Figure 2.19 Distributions of queue lengths at different intersection approaches

Performance under the light volume scenario (Scenario 3)

Figures 2.20-24 show the freeway's lane speeds and the distributions of queue lengths under the relatively low freeway traffic scenario. As expected, under such a low-volume traffic scenario, all three control systems can maintain average lane speeds above 40 kph (see Figure 2.20, Figure 2.21, and Figure 2.22). Figure 2.23 shows the speed comparisons of the outermost lane (i.e., lane 1) with all three control strategies under this scenario. The MOEs for such a traffic scenario can further support the advantage of always coordinating the ramp metering control with its neighboring intersections which accommodate traffic flows to the freeway. As with the previous two scenarios, the intersection queue lengths with the proposed RAF-ramp under Scenario 3 are constantly shorter than the link lengths (see Figure 2.24).

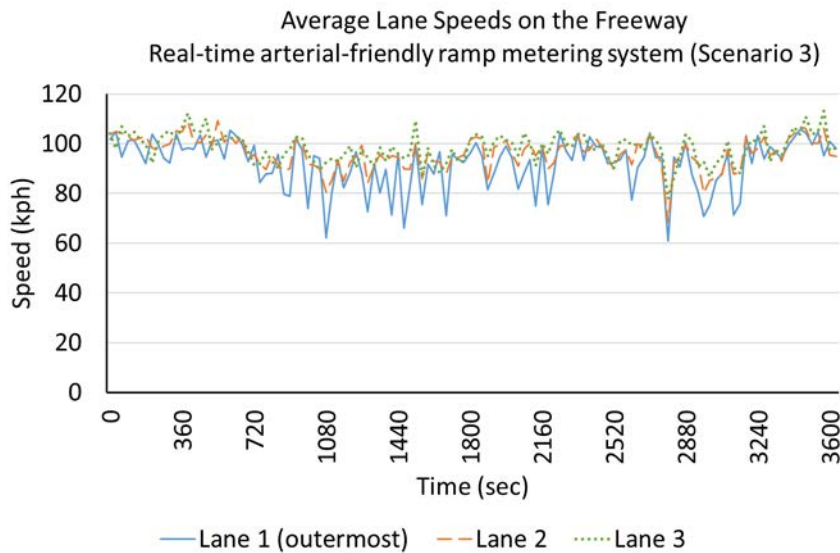


Figure 2.20 Average lane speeds turning on the freeway's merging segment under RAF-ramp control

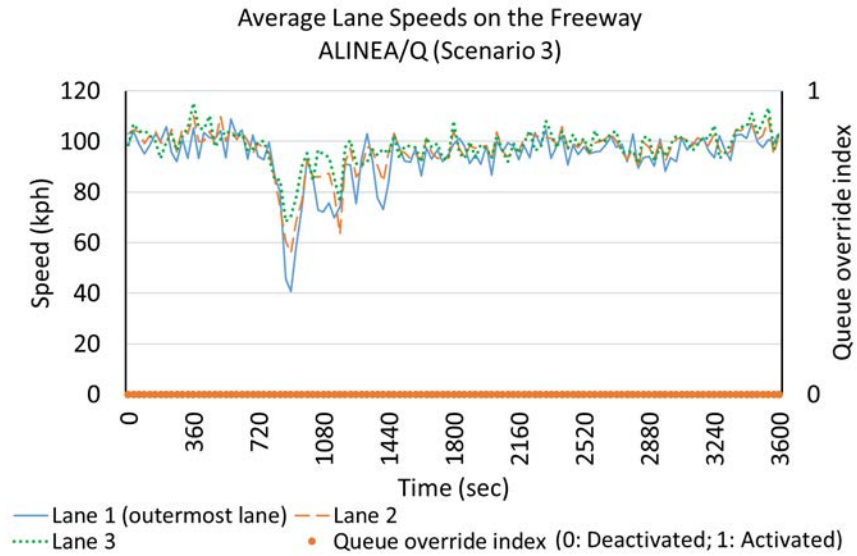


Figure 2.21 Average lane speeds on the freeway's merging segment under ALINEA/Q control

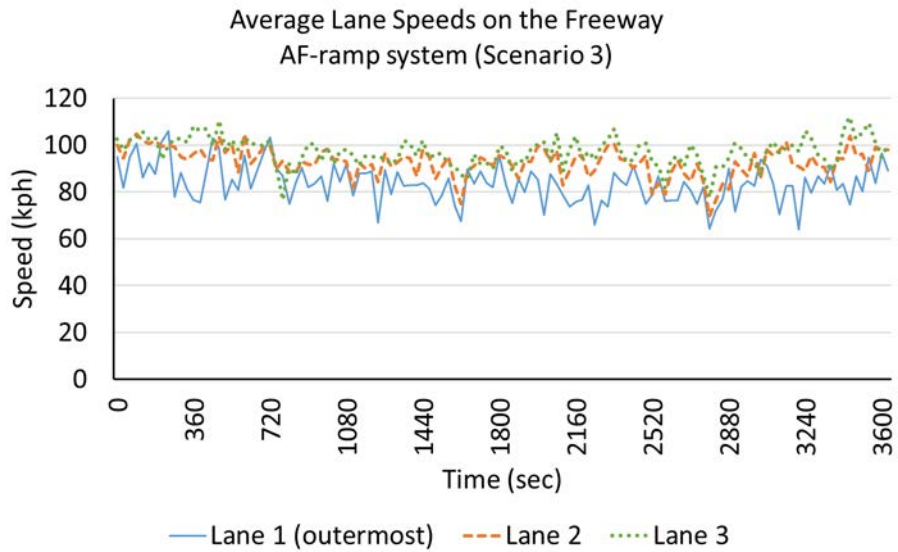


Figure 2.22 Average lane speeds on the freeway's merging segment under the AF-ramp system

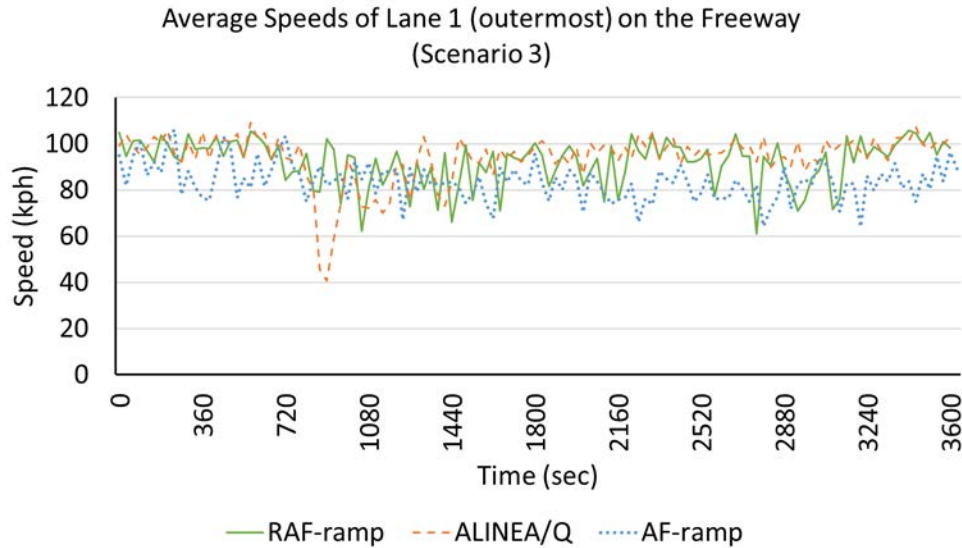


Figure 2.23 Comparison of average speeds of lane 1 (outermost) on the freeway's merging segment

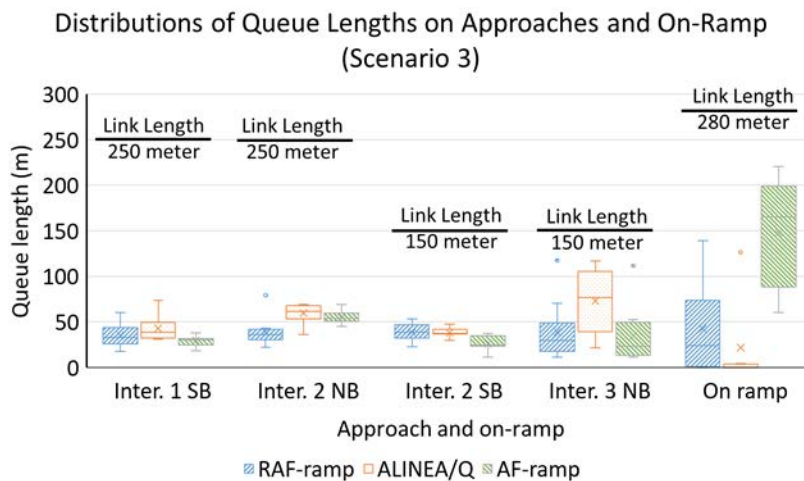


Figure 2.24 Distributions of queue lengths at different intersection approaches

Network-wide delay under all volume scenarios

Table 2.10 shows the total delays of the entire network under the control systems with the two real-time and one pre-timed ramp metering strategies. The results demonstrate that the proposed RAF-ramp outperforms the other two controls in all three scenarios, especially in medium- and high-volume scenarios (i.e., Scenarios 1 and 2). Such improvement mainly comes from the freeway mainline, as evidenced by the total delays on the freeway mainline and on-ramp under Scenarios 1 and 2, as shown in Figure 2.25. For example, under Scenario 2 of high-volume traffic conditions, the RAF-ramp system can achieve up to 63.27% and 67% improvements, compared to ALINEA/Q and AF-ramp, respectively. In the same scenario, the total delay on the freeway mainline under RAF-ramp control is 8.1 veh-hours, significantly lower than those of ALINEA/Q and the AF-ramp system (i.e., 115.4 and 118.5 veh-hours, respectively), as shown in Figure 2.25 (b).

Moreover, the benefits of the RAF-ramp system tend to increase with the freeway's traffic volume. As shown in Table 2.10, when freeway volume increases by 5% (i.e., from Scenario 1 to Scenario 2), the total delay under the proposed RAF-ramp increases by 28.96% (from 46.83 veh-hours in Scenario 1 to 60.39 veh-hours in Scenario 2), considerably lower than the increments of 176.8% and 167.15% with the ALINEA/Q and the AF-ramp controls, respectively.

In brief, the proposed RAF-ramp system, by optimally coordinating the ramp metering control with signals at its neighboring intersections, outperforms the pre-timed version control system (i.e., AF-ramp system) and the ALINEA/Q, designed solely for optimizing the ramp metering cycle, with respect to the total network delays, total throughput, and freeway speeds.

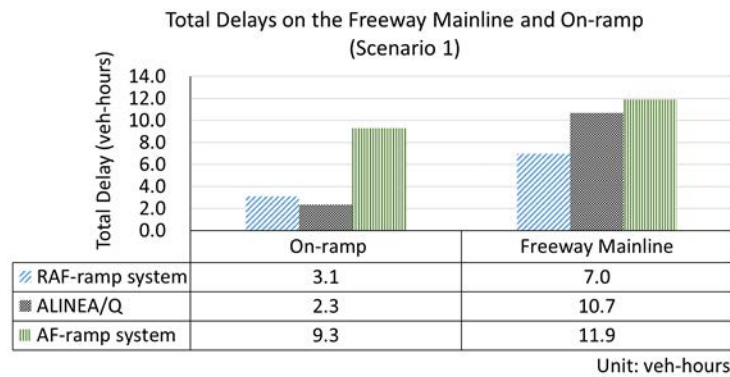
Table 2.10 Total delays of the Proposed RAF-ramp, ALINEA/Q, and AF-ramp

Unit: veh-hours

Control strategy	Scenario			Increment ¹ (Scenarios 2 vs. 1)
	1	2	3	
RAF-ramp system	46.83	60.39	40.33	28.96%
ALINEA/Q	59.40	164.42	43.15	176.80%
AF-ramp system	68.50	183.0	51.30	167.15%
Improvement ²				
Compare w/ ALINEA/Q	21.16%	63.27%	6.54%	
Compare w/ AF-ramp	31.64%	67.00%	21.38%	

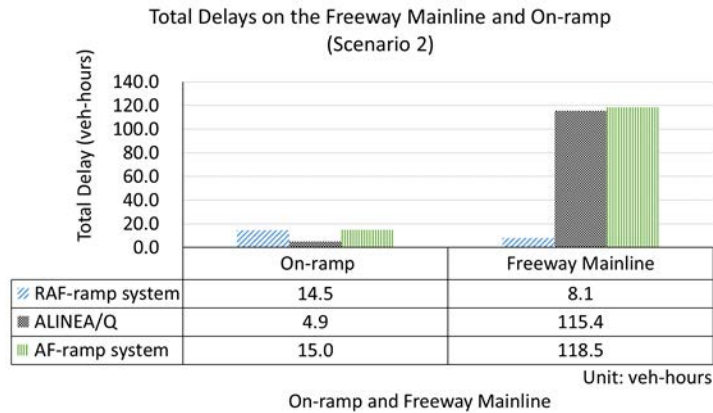
¹ Increment = (total delay of the control approach under Scenario 2 - total delay of the control approach under Scenario 1)/(total delay of the control approach under Scenario 1)*100%

² Improvement = (total delay of the compared control approach - total delay of the proposed RAF-ramp system)/(total delay of the compared control approach)*100%



On-ramp and Freeway Mainline

(a)



(b)

Figure 2.25 Total delays on the freeway mainline and on-ramp under two different controls (a) Scenario 1 (b) Scenario 2

2.6 Closure

To transform the relationship between motorists on freeways and neighboring arterials from competition to coordination in contending with recurrent congestion in interchange areas due to excessive on-ramp volume, this study has proposed the RAF-ramp control system. The system aims to maximize the total throughput for both the freeway segment and arterial intersections within the same control area with optimally coordinated dynamical ramp metering and multi-path local signal progression control. To sufficiently respond to the freeway traffic dynamics while maintaining the stability of local signal control, the proposed system executes systemwide updates of both the ramp metering cycle and coordinated signal plans if the local dynamic ramp control is predicted to cause queue overflows.

The systemwide optimization module, by integrating the predicted freeway traffic conditions from the LGB module with the coordinated signal and ramp relations in the AF-ramp models, can concurrently produce the optimized ramp metering cycle and neighboring intersections' cycle length, green splits, phase sequences, and offsets, with the objective to maximize the total system throughput without ramp queue spillback.

The results of extensive simulation experiments have confirmed that, under three experimental traffic scenarios, the proposed system can produce optimal control strategies that effectively utilize the freeway's weaving capacity and coordinate neighboring intersections' signal controls to prevent on-ramp queue spillbacks. The results of performance comparison with the AF-ramp model provide evidence of the necessity of adopting real-time control when traffic volume is unstable. Additionally, the comparison with a real-time ramp control model further supports the need to integrate the intersections that feed traffic to the on-ramp into the same control system. With optimized coordination between the ramp metering cycle and local signal plans, an interchange can effectively keep its freeway segment's throughput at the weaving capacity while ensuring no ramp overflows as its arriving traffic responsively regulated by the local signals.

Further studies will focus on expanding the proposed system to account for the impacts of off-ramp flows on congestion affecting both the freeway and its neighboring arterial, ultimately developing a full interchange-based real-time traffic control system. Another natural extension of this study is to expand the coordinated local ramp and intersection controls to a corridor-wide

traffic management system that covers multiple freeway segments and local arterials significantly impacted by the on- and off-ramp traffic.

Chapter 3 Integrated Real-Time Interchange Control System for Freeway Ramps and the Connecting Arterial

3.1 Introduction

Contending with recurrent traffic congestion on major freeway corridors has long been a top priority of the transportation community. According to the most recent Urban Mobility Report (Texas A&M Transportation Institute, 2021), traffic congestion has caused urban Americans to travel an extra 8.7 billion hours and consume an additional 3.5 billion gallons of fuel at a cost of \$190 billion in 2019. Furthermore, over 50% of congestion in the urban areas occurred on freeways. Freeway congestion has become significantly more severe during the past decade despite the tremendous efforts devoted by various highway agencies on traffic controls and management.

Freeway bottlenecks are often formed around interchange areas due to their excessive entering and exiting flows during peak hours. Figure 3.1 demonstrates a freeway interchange with representative geometric conditions, as well as three closely spaced intersections on its connecting surface street. As shown in the figure, such merging and diverging segments on the freeway mainline with both high exiting and ramp merging flows may often suffer three major recurrent issues: 1) off-ramp queue spillbacks to the freeway mainline, 2) frequent lane change maneuvers triggered by the exiting and entering flows at the merging/diverging area resulting in speed reduction and capacity drop, and 3) on-ramp queue spillback (probably caused by the ramp metering) to the connecting urban arterial, causing potential intersection queue spillovers. The impacts of these issues are often closely correlated with each other and may aggravate each other when any aspect has not been sufficiently managed, resulting in a major bottleneck. For example, the potential capacity drop at the on-ramp area would cause the congestion to propagate to the upstream segments and worsen the consequences of off-ramp queue spillbacks. Recognizing the critical role of interchange traffic controls on maintaining efficient freeway operations, the traffic community over the past decades has focused most research tasks regarding mitigation of corridor congestions on the following two most critical areas: on-ramp metering and off-ramp coordinated signal control.

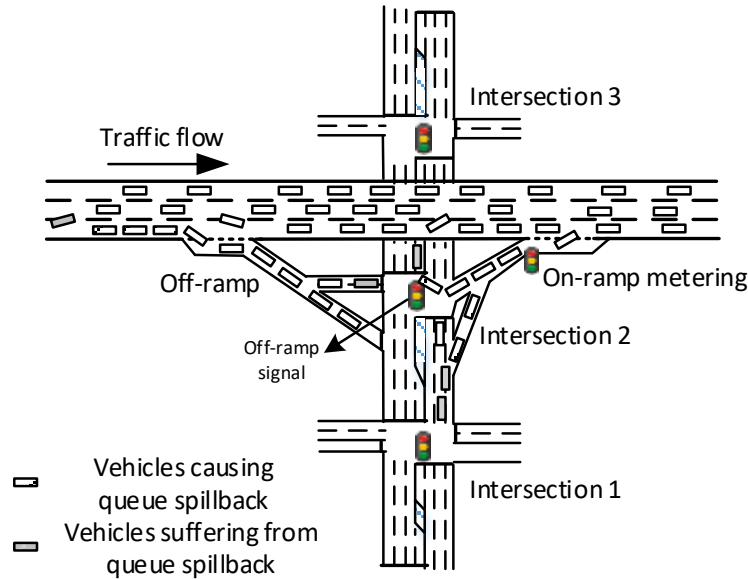


Figure 3.1 A freeway interchange with an on-ramp, an off-ramp, and a connecting arterial

Among the large body of literature for traffic control within the interchange area, on-ramp metering is one of the most extensively explored strategies. Such methods are designed to regulate excessive on-ramp entering volumes so as to prevent the formation of a bottleneck on the freeway's weaving segment due to extensive merging and lane-changing maneuvers. Over the past decades, the traffic community has proposed various types of ramp metering control strategies, including local metering control (Papageorgiou et al., 1991; Zhang and Ritchie, 1997; Smaragdis et al. 2004; Gomes and Horowitz, 2006; Wang and Papageorgiou, 2006), coordinated ramp metering control (Kotsialos et al., 2002; Papamichail et al., 2010a; Papamichail et al., 2010b; Ghods et al., 2010; Geroliminis et al. 2011, Zhao et al., 2011; Chow and Li, 2014; Agarwal et al., 2015), integrated ramp metering and variable speed limit (VSL) controls (Hegyi et al., 2005; Carlson et al., 2010a; Carlson et al., 2010b; Frejo and Camacho, 2012; Carlson et al., 2014; Li et al., 2017), cooperated ramp metering and local traffic controls (Head and Mirchandani, 1997; Tian et al., 2005; Tian, 2007; Cheng and Chang, 2021), and collaborated ramp metering control and route guidance strategy (Kotsialos et al., 2002; Karimi et al., 2004; Liu et al., 2011; Pasquale et al., 2017). However, most such ramp metering controls are designed mainly to benefit the freeway, and thus often result in excessive on-ramp queues during peak hours. Such resulting queues due to high on-ramp volume, if not effectively managed, will inevitably spill back to the neighboring intersections and even cause gridlocks on the local arterial.

A standard practice to cope with the issue of excessive on-ramp queues is to pause the ramp control or to increase the metering rate when the detected on-ramp queue length exceeds a pre-defined threshold. Doing so frequently during peak hours will, however, defeat the purpose of implementing the ramp metering control, or render it ineffective in preventing the freeway from being plagued by local congestion. To balance the benefits between freeway mainline and the surrounding arterial traffic, some studies (Chang et al., 2020; Cheng and Chang, 2021) have developed an arterial-friendly local ramp metering (AF-ramp) strategy that can maximize the network throughput and avoid arterial link queue spillbacks with an optimized ramp metering rate

and signal plans at nearby intersections for fixed-time or time-of-day uses. However, the off-ramp queue impacts on freeway mainline traffic have not been considered in their control approaches.

As another major category of methods for freeway interchange control, the off-ramp signal control is developed to regulate the freeway's exiting volumes to the arterial so that such flows can merge smoothly with local traffic. In the design of such a signal plan, without fully accounting for the off-ramp spillback impacts on the freeway, may often yield insufficient green time or excessive waiting time to the off-ramp flows, and cause off-ramp queues to spill back to the freeway mainline and further result in its substantial speed reduction. In the large body of freeway control literature, very few studies (Li et al., 2009; Lim et al., 2011; Zhao and Liu, 2016; Yang et al., 2014; Yang et al., 2018; Chang et al., 2020; Chen et al., 2021a; Chen, 2021) have proposed methods to prevent off-ramp queues from spilling back to the freeway mainline with the optimized off-ramp signal design. For example, Chen et al. (2021a) have developed an integrated off-ramp control model that incorporates the impact of ramp queue spillback in the design of the off-ramp intersection's signal plan.

Note that both the aforementioned on-ramp control and the off-ramp control strategy have distinct objectives and are often implemented independently without cooperating with each other, despite the fact that their effectiveness both depend on the optimization of the connecting intersection's signal. Conceivably, to achieve the most desirable control effectiveness within the entire interchange area, the ramp metering system and the signal design of the connecting arterial should coordinate with each other, thus raising a need for an integrated interchange control system that can benefit the operation of both on-ramp and off-ramp segments.

Moreover, most aforementioned studies for either arterial friendly on-ramp controls or off-ramp controls remain at the off-line level and cannot effectively respond to traffic fluctuations, thus rendering it difficult to reach the desirable effectiveness under practical traffic conditions. Over the past decades, various traffic-responsive control methodologies have been proposed (Masher et al., 1975; Jacobson et al., 1989; Papageorgiou et al., 1991; Papageorgiou et al., 1997; Smaragdis and Papageorgiou, 2003; Smaragdis et al., 2004; Frejo and De Schutter, 2018) to respond to the fluctuation of traffic patterns in a timely manner.

To summarize, the fundamental issue of coordinating real-time freeway and local traffic flows in the vicinity of its interchanges, with on-ramp control, off-ramp control, and arterial signal optimization, so as to maximize the total benefits of both the freeway and local users, has yet to be addressed. In view of this, this study develops an Integrated Real-time Interchange Control (IRIC) system to concurrently mitigate the freeway's traffic congestions and also minimize negative impacts from various causes on the nearby local arterials. The proposed system is capable of:

- Responding to time-varying traffic volumes entering the interchange area from both the freeway mainline and all feeding arterial links in a timely manner with proactive ramp metering and signal controls based on the embedded lane-group-based traffic predicting module;
- Monitoring the traffic state for efficient and reliable decisions regarding the implementation of either a dynamic adjustment of metering cycles alone or a system-wide update to concurrently re-optimize ramp metering and signal plans for all nearby intersections;
- Maximizing the total throughput for both the freeway and arterial links within the interchange area based on the real-time detected flows;

- Preventing off-ramp queues from spilling back to the freeway mainline by optimizing the signal plan at the connecting intersection;
- Avoiding on-ramp queue spillovers to neighboring local streets by coordinating intersection signal plans with ramp metering control; and
- Optimizing the signal plan for each nearby intersection to ensure the absence of either turning bay spillover that may block the local through traffic or create queue spillback to the upstream intersections.

3.2 Integrated Real-Time Interchange Control (IRIC) System

A real-time traffic control system with the capabilities above shall embed several mechanisms and modules to ensure: 1) the control system can be activated based on traffic conditions; 2) the control strategies can be updated in response to traffic evolutions; 3) the computational effectiveness can satisfy real-time control needs; and 4) the system can be deactivated appropriately. Figure 3.2 shows the operational flowchart of the proposed IRIC system, which mainly consists of the following three stages: 1) initialization and assessment; 2) projection of traffic evolution patterns and selection of the initial ramp metering cycle; and 3) dynamic execution of the integrated ramp and local signal controls. Stage 1 functions to first determine whether the real-time control should be activated based on the prevailing traffic volume and that estimated using the OQI and LGB models. To ensure the correct selection of the control strategy, Stage 2 prepares the required inputs for determining the necessity of system-wide optimization by using the LGB model to search for a preliminary optimal ramp metering cycle length and calculating the trend of traffic evolution. Stage 3 will first determine the optimization type (i.e., ramp metering optimization or system-wide optimization) and proceed with the corresponding module. Technical details and formulations required in each stage are introduced in the section below.

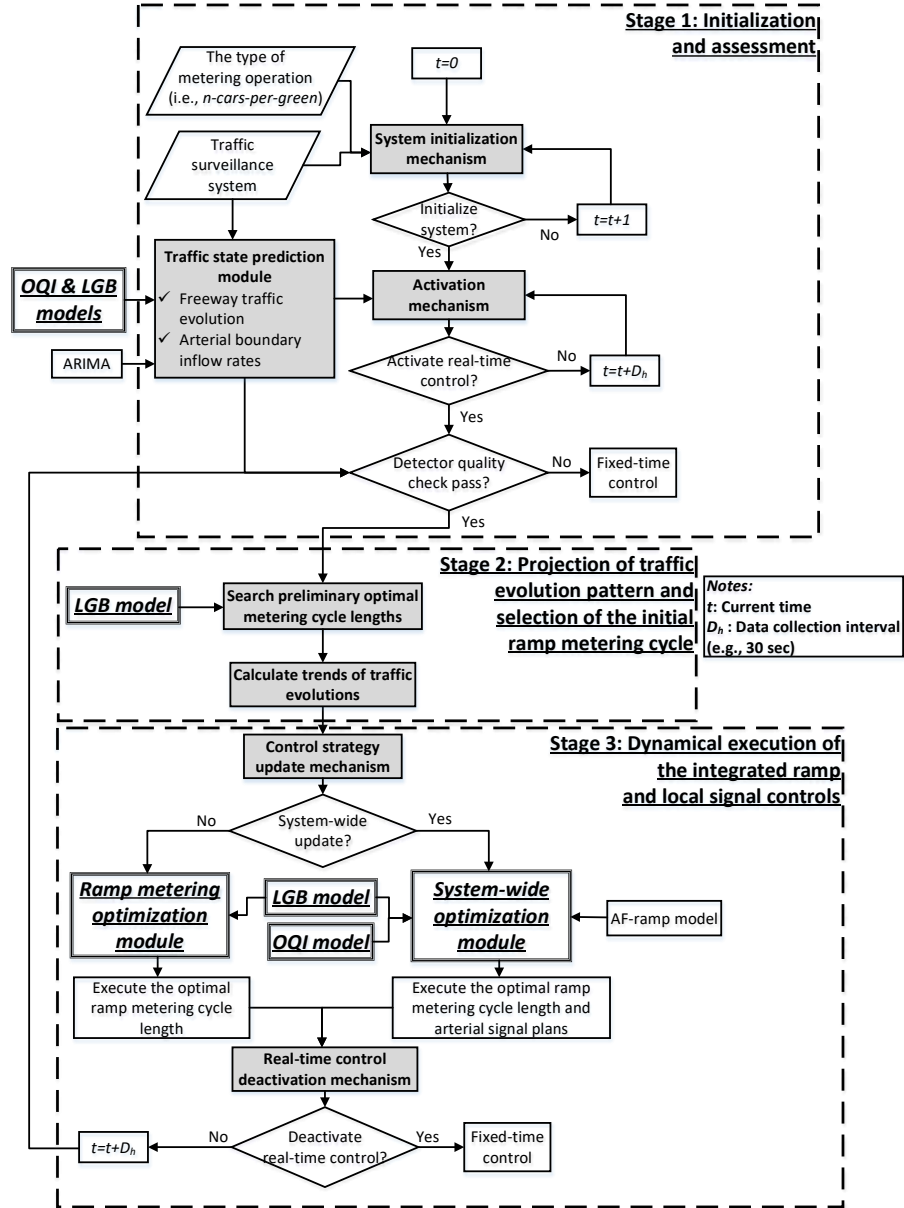


Figure 3.2 The operational flowchart of the proposed IRIC system

Note that the off-ramp queue impact (OQI) and lane-group based (LGB) models proposed by Chen et al. (2021a) and Chen et al. (2021b) are adopted in the IRIC system to predict the freeway's traffic evolution and for timely execution of the system-wide and ramp control optimization modules, respectively. The OQI model (Chen et al., 2021a) is designed to perform the estimation of the off-ramp queue length, the frequencies of the discretionary and mandatory lane-changing activities due to off-ramp queue spillovers, and their resulting impacts on the freeway's traffic conditions. The inputs of the OQI model are the upstream arriving lane flow rates of the freeway mainline and the exiting split ratios at each time interval. With those inputs, the model can predict short-term off-ramp queue lengths, lane speeds, and lane flow rates through the following steps: 1) estimating the number of intended lane-changing vehicles in each lane; 2) computing the available roadway space for successful lane changes and the length of the off-ramp queue

spillback; 3) computing the impacts of the lane changes on the mainline' traffic speed; and 4) computing the density and flow rate of each lane.

In addition, the LGB model (Chen et al., 2021b) is designed with the functions of 1) capturing the impact of the lane-changing behaviors on the speeds of both the target and the departing lanes; 2) accounting for the impact of on-ramp merging vehicles on the freeway segments upstream and downstream of the on-ramp; and 3) capturing the complex interrelations between the freeway traffic state and the lane-changing maneuvers. Such information will serve as the basis for determining the on-ramp metering settings in the proposed IRIC system. The inputs of the LGB model include upstream arriving flow rates on freeways, on-ramp flow rates, and density ratios among lanes for determining lane change frequencies. When applying the LGB model, one shall first divide the freeway segment into several sub-segments and then separate each sub-segment into several lane groups based on the similarities of traffic dynamics among lanes. For each segment, the LGB model will first determine the numbers of lane changes between neighboring lane groups. After the frequencies of different lane-changing activities have been estimated, the LGB model has specified an extra term to account for the effect of the speed differences between the departure and receiving lane groups on the lane-changing activities over each lane group. Such information can be combined with the specified relaxation, convection, and anticipation terms to collectively determine the speeds of all lane groups. The relaxation term functions to allow the speed to deviate from its equilibrium value; the convection term is designed to reflect the continuity of traffic conditions between two consecutive lane groups; and the anticipation term is specified to reflect the perceivable impacts of the downstream connected lane group's traffic conditions on the speed of drivers in the subject lane group. For the lane group connected to the on-ramp, an extra term is added to the speed function to capture the effects of mandatory lane changes by merging vehicles. Given the estimated speed for each lane group, one can directly employ the calibrated speed-density and speed-flow relations to compute the estimated flow rate and density for each lane group and the entire freeway segment. The outcomes of the model are speeds, flow rates, and densities of each freeway segment at each time interval (Chen et al., 2021b).

On freeway mainline segments near interchanges, the frequency of discretionary lane changes triggered by existing or entering flows is one of the critical factors influencing levels of capacity drops. The higher the frequency of discretionary lane changes is, the higher capacity drops. Both traffic models, OQI and LGB models, possess functions to estimate the number of such lane changes. Equation 3.1 and Equation 3.2 below show the discretionary lane change functions in the OQI and LGB models.

$$y_{j,l}(k) = \left(\frac{\exp(\bar{v}(k) - v_j(k) - \mu_1)}{1 + \exp(\bar{v}(k) - v_j(k) - \mu_1)} \right)^{\beta_1} \left(\frac{\exp(v_l(k) - v_j(k) - \mu_2)}{1 + \exp(v_l(k) - v_j(k) - \mu_2)} \right)^{\beta_2} \left(\frac{(\rho^{jam} - \rho_l(k))}{|v_l(k) - v_j(k)| + \xi} \right)^{\beta_3} e^{\delta\beta_4} \quad (3.1)$$

where, $y_{j,l}(k)$ denotes the number of discretionary lane changes from lanes j to l at time k at the freeway mainline segment upstream of off-ramps; $\bar{v}(k)$ is average speed across all freeway's travel lanes at time interval k ; $v_j(k)$ denotes speed on lane j at time interval k ; μ_1 is the average threshold of speed differences between the subject lane and entire cross section from sample lane-changing drivers; μ_2 is the average threshold of speed differences between subject and target lanes from sample lane-changing drivers; ρ^{jam} is jam density; $\rho_l(k)$ denotes the density of lane l at time interval k (prior to experiencing the lane changes by vehicles); $\delta = 1$, if changing to the right; $\delta =$

0, otherwise; ξ is a very small value to prevent the denominator of the term, $(\rho^{jam} - \rho_l(k))/(|v_l(k) - v_j(k)| + \xi)$, from equaling 0; and $\beta_1, \beta_2, \beta_3$, and β_4 are parameters.

$$n_{i,j,j+1}(k) = \begin{cases} \min(L_i \rho_{i,j}(k), \eta \lambda_{i+1,j} \lambda_{i+1,j+1} L_{i+1} \frac{\rho_{i+1,j}(k) - \rho_{i+1,j+1}(k)}{\lambda_{i+1,j} + \lambda_{i+1,j+1}} \\ , (\rho^{jam} - \rho_{i,j+1}(k)) L_i), \text{ if } \rho_{i+1,j}(k) > \rho_{i+1,j+1}(k) \\ 0, \text{ otherwise} \end{cases} \quad (3.2)$$

where, $n_{i,j,j+1}(k)$ is the number of vehicles changing from lane group j to $j+1$ in segment i at time k ; L_i is the length of segment i ; $\rho_{i,j}(k)$ denotes density of lane group j in segment i at time k (prior to experiencing the lane changes by vehicles); $\lambda_{i,j}$ is the number of lanes in lane group j in segment i ; and η is the parameter to reflect the characteristics of driving populations and their reactions to the perceived on-ramp volume.

In Equation 3.1, according to the sensitivity analysis conducted in the previous study (Chen, et al., 2021a), decreasing β_1, β_2 , and β_3 will increase the percentage of drivers intending to conduct discretionary lane changes to faster lanes, and consequently cause speed reduction on lanes 4 and 5, but not on the lane outflow rates. By contrast, the lane speeds and outflow rates are relatively insensitive to different values for β_4 . Such results reveal that drivers generally prefer to stay on the left lane within the off-ramp weaving segment, especially during peak hours, even though their intentions to change to the right lane of the faster-speed lane may increase with the increased specified value for β_4 .

For Equation 3.2, a decrease in η (i.e., decreasing the willingness of lane changes from the outer to the inner lane groups at the freeway mainline segment upstream of the on-ramp) will result in a reduction of the average speed of lane groups at the freeway mainline segment. Furthermore, due to the interdependent relation between consecutive lane groups, the average speeds of lane groups in the further downstream segments will also decrease (Chen, et al., 2021b). For a more detailed discussion, please refer to the studies by Chen et al. (2021a) and Chen et al. (2021b).

The control boundaries for a typical freeway interchange are shown in Figure 3.3. The proposed system would apply to an interchange where its off-ramp is at the upstream of the on-ramp, as shown in Figure 3.3.

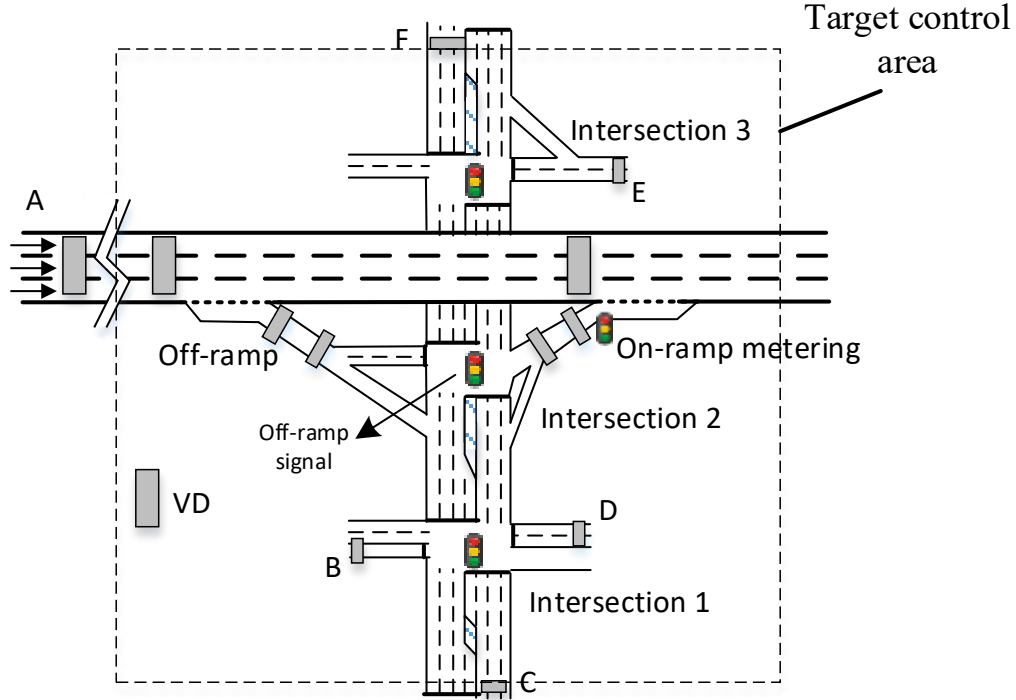


Figure 3.3 Control boundaries and the locations of vehicle detectors

For real-time monitoring of traffic conditions and the embedded models' performance, the proposed IRIC system would require reliable vehicle detectors (VDs) to be deployed at the following locations (see Figure 3.3): 1) at the upstream end of each intersection approach around the boundary of the target control area for collecting entering flow rates; 2) at the on-ramp/off-ramp for detecting flow rates and the queue lengths; and 3) at the freeway mainline segments right upstream of the off-ramp and on-ramp to monitor mainline traffic conditions.

Stage 1 – Initialization and assessment

At this stage, the proposed system shall monitor the target area's traffic conditions in a real-time manner and, at each time interval, determine whether to activate the real-time interchange control operations. Concurrently with the traffic monitoring function, the proposed system shall also constantly assess detectors' data quality and reliability. Some well-established methods for such needs can be found in the literature (Achillides and Bullock, 2004; Lu et al., 2014).

System initialization mechanism

Both OQI (Chen et al., 2021a) and LGB (Chen et al., 2021b) are, by nature, macroscopic online simulation models; they thus need initial roadway traffic conditions based on sensor data for system initialization. Such initial traffic states are typically selected from a time point exhibiting a low and stable traffic pattern ahead of the peak hours.

Traffic state prediction module

At current time interval t , the system shall employ the OQI (Chen et al., 2021a) and LGB (Chen et al., 2021b) models to predict the flow rates on both freeway segments upstream of off-ramps and on-ramps over the next N time intervals (i.e., $t+1$ to $t+N$), denoted as $W_t^E(t+n)$ and $W_t^O(t+n)$, respectively, where, $n = 1, \dots, N$. Therefore, the expected flow rate on the freeway

segment upstream of the off-ramp for a projected time instant k , denoted as $\bar{W}^E(k)$, can be viewed as the average of all flow rates predicted from the previous $k-N$ intervals to the current interval t . Such a process is expressed mathematically as below:

$$\bar{W}^E(k) = \frac{W_{k-N}^E(k) + W_{k-N+1}^E(k) + \dots + W_t^E(k)}{N - (k - t) + 1} \quad (3.3)$$

Figure 3.4 shows an example where the duration of each time interval is 30 sec and $N=10$ at the current time of 7:00:00 AM. The proposed IRIC system will produce the projected traffic states up to 7:05:00 AM at every time unit of 30 seconds. Hence, following the same prediction exercise, the system with the OQI model (Chen et al., 2021a) up to 7:04:30 AM will have ten predicted traffic flow rates at the upstream segment of the off-ramp for the interval of 7:05:00 AM, i.e., $W_{7:00:00}^E(7:05:00)$, $W_{7:00:30}^E(7:05:00)$, ..., $W_{7:04:30}^E(7:05:00)$. Then, the system will apply the ten predicted results with Equation 3.3 to compute the expected flow rate for the 7:05:00 AM interval (i.e., $\bar{W}^E(7:05:00)$). Following the same logic, one can compute the expected flow rates for the following nine time intervals (i.e., 7:05:30 AM to 7:09:30 AM).

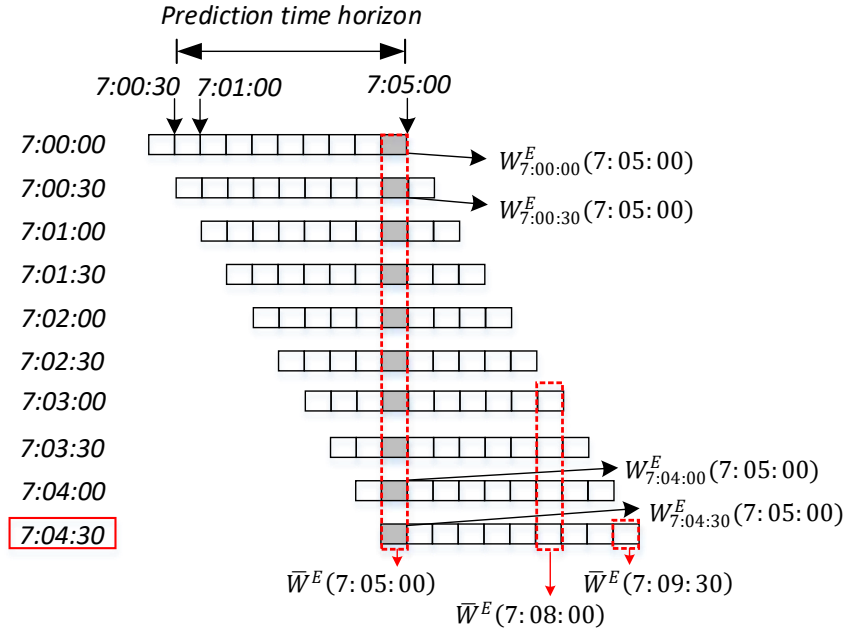


Figure 3.4 Example of calculating expected flow rate for the projected time interval

After applying the process above and obtaining a series of predicted flow rates over the projected time horizon, one can then estimate the trend for the expected flow rates, using all obtained $\bar{W}^E(k)$, where $k = t+1, t+2, \dots, t+N$, with Equation 3.4, where the slope, a_1 , indicates the evolution trend of $\bar{W}^E(k)$ over the future N intervals.

$$f(k) = a_1 \cdot k + b_1 \quad (3.4)$$

One can predict the flow rates on the freeway segment upstream of the on-ramp, $\bar{W}^O(k)$, over the projected time horizon with the same logic, using the data obtained from the on-ramp detector, and calibrate the slope of the resulting trend line as a_2 .

Activation mechanism

After initialization, this system will then determine whether or not the real-time control should be activated based on the predicted and detected freeway's traffic states on the freeway

segments upstream of the off-ramp and on-ramp, as shown in Table 3.1. The purpose of considering both traffic predictions and detections in the activation mechanism is to enhance system reliability by providing dual sources and avoid the possibility of the system not acting in time due to prediction bias. Specifically, when the conditions in Steps 1 and 2 are satisfied, the entering volume is expected to reach a level that may cause breakdown according to historical data and is unlikely to decrease in the next several intervals. To increase the reliability of the activation mechanism, detected volumes in the past several intervals are also examined in addition to the predicted volume, as specified in Steps 3 and 4.

Table 3.1 Assessment process for activating the real-time control

Step 1
At time t ,
If (at least I_1 percent of $\bar{W}^E(k)$ in the next 5 min $> \gamma_1$) and ($a_1 \geq 0$)
then go to Step 5;
else go to Step 2;
Step 2
If (at least I_2 percent of $\bar{W}^O(k)$ in the next 5 min $> \gamma_2$) and ($a_2 \geq 0$)
then go to Step 5;
else go to Step 3;
Step 3
If (at least I_3 percent of the detected flow rates on the freeway segment upstream of the off-ramp over the past 5 min $> \gamma_3$)
then go to Step 5;
else go to Step 4;
Step 4
If (at least I_4 percent of the detected flow rates on the freeway segment upstream of the on-ramp over the past 5 min $> \gamma_4$)
then go to Step 5;
else go to Step 6;
Step 5
Stop and activate real-time control;
Step 6
$t=t+D_h$ and go to step 1.

Note: a_1 presents the slope of the trend line of $\bar{W}^E(k)$ in the next 5 min; a_2 is the slope of the trend line of $\bar{W}^O(k)$ in the next 5 min; I_i are pre-selected percentages and are set to 50% in this study; γ_i are pre-defined thresholds and should be calibrated for each specific site based on the historical data; D_h is the data collection interval (e.g., 30 sec)

Stage 2 – Projection of traffic evolution pattern and selection of the initial ramp metering cycle

Search preliminary optimal metering cycle lengths

To ensure that Stage 3 will have sufficient information to decide whether or not the system shall conduct a system-wide update or ramp metering re-optimization only, the primary function at this stage is to conduct a preliminary estimation of the cycle length for ramp control for the projected interval of next $(t + 5)$ min, given the freeway entering flow rates and arterial signal plans at current time interval t . Since the metering rate is derived using highly nonlinear formulations in the LGB model, solving such a problem using mathematical programming is not realistic. Therefore, the authors have proposed the search algorithm in Table 3.2 to ensure that one can find an optimal preliminary solution in a sufficiently short period (i.e., less than one second). Specifically, the estimated ramp metering cycle length, given a prespecified n-car-per-green operational guide, is expected to yield the maximum freeway throughput. Such estimated ramp metering cycle lengths may not be eventually implemented but would be a good approximation to the values to be applied.

Table 3.2 Algorithm for the search of the estimated preliminary cycle length for ramp metering control

At the current time t ,

Step 1
Set $t_a = t$ and metering cycle length $(C_t) = C_{o,min}$

Step 2
Predict *freeway throughput* (V_{t_a, C_t}^F) at the downstream of the on-ramp of the period (t_a) to ($t_a + D_h$) with a given metering cycle length, C_o , by the **LGB model**.

Step 3
If $C_o < C_{o,max}$
 then $C_o = C_o + I$ **and** go to Step 2.
 else go to Step 4.

Step 4
Choose the metering cycle length with maximal freeway throughput as the preliminary optimal cycle length (\hat{C}_{ta}) for the period (t_a) to ($t_a + D_h$).

Step 5
If $(t_a - t) < 300 \text{ sec}$
 then set $t_a = t_a + D_h$ **and** $C_o = C_{o,min}$ **and** go to Step 2
 else stop and output the optimal metering cycle lengths

Note: $C_{o,min}$ is a prespecified lower bound of the metering cycle length; $C_{o,max}$ is a prespecified upper bound of the metering cycle length; and D_h denotes data collection frequency (i.e., 30 sec).

Calculate trends of traffic evolutions

In addition, since the two optimization modules in Stage 3 will optimize the control strategies based on the traffic conditions in the next 5 min, primary information to be produced from Stage 2 at each time interval in real-time includes: 1) the predicted freeway exiting flow rates over the next 5 min; 2) the predicted flow rates on the freeway segment upstream of the on-ramp in the next 5 min; 3) the predicted arterial boundary inflow rates in the next 5 min; 4) the differences between the detected and predicted inflow rates through the arterial's control boundaries over the past 5 min; and 5) the detected occupancy at the on-ramp and off-ramp over the past 5 min.

Stage 3 – Dynamical execution of the integrated ramp and local signal controls

Control strategy update mechanism

To avoid adjusting local signal control settings frequently, the IRIC system only updates local signal plans when needed. With the estimation of initial metering cycle lengths that are obtained in the previous stage, the proposed system at this stage will first determine if a system-wide update (i.e., concurrently update the ramp metering cycle length and arterial signal plans) or only the ramp metering update should be executed, as shown in Figure 3.5. The system will assess whether the estimated off-ramp queues, on-ramp queues or inflow rates would justify the need for a system-wide control. The assessment will be based on the estimation of these constantly evolving variables based on detector data and the estimated preliminary ramp metering cycle length. The detailed procedure for such assessments is demonstrated in Table 3.3 to 3.5. Just as the activation mechanism shown in Table 3.1, the detections and predictions are adopted in these assessment procedures to ensure that the system would not be affected by prediction bias.

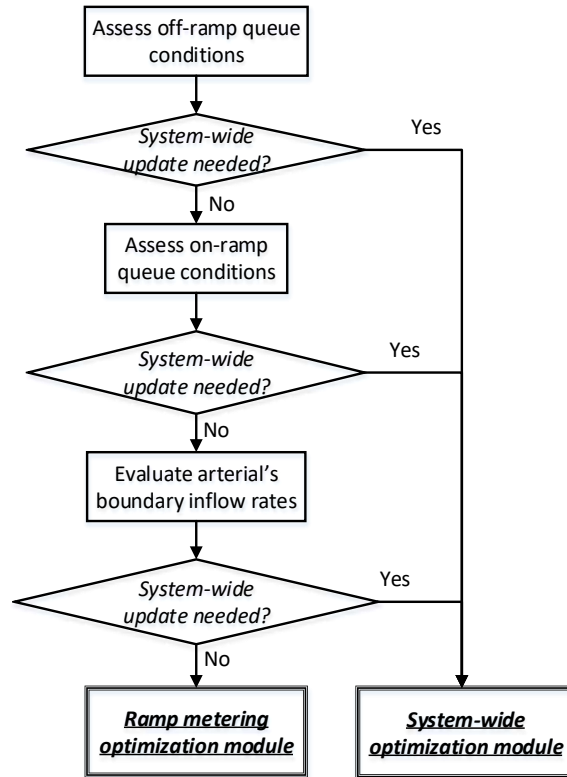


Figure 3.5 Flowchart of the system-wide update mechanism

Table 3.3 Procedure for assessing the off-ramp queue conditions

Step 1

If (at least I_5 percent of off-ramp queue lengths predicted for the next 5 min > length of the off-ramp) and ($S(\text{predicted freeway exiting flow rates}) \geq 0$)
 then go to Step 4;
 else go to Step 2;

Step 2

If ($S(\text{the predicted freeway exiting flow rates}) \geq 0$) and ($S(\text{detected occupancy rates of the upstream detector of the off-ramp}) \geq 0$) and ($\sigma_u^E(t - n_1 \cdot D_h) \geq 25\%$, $n_1 = 0$ to 1) and ($\sigma_m^E(t - n_2 \cdot D_h) \geq 25\%$, $n_2 = 0$ to 5)
 then go to Step 4;
 else go to Step 3;

Step 3

If ($S(\text{detected occupancy rates by the middle detector placed on the off-ramp segment}) < 0$) and ($S(\text{predicted freeway exiting flow rates}) \leq 0$)
 then go to Step 4;
 else go to Step 5;

Step 4

Stop and output "system-wide update needed."

Step 5

Stop and output "system-wide update not needed."

Note: $S(\cdot)$ presents the slope of the trend line of the target variable; $\sigma_u^E(t)$ denotes the occupancy rate of the upstream detector on the off-ramp at time t ; $\sigma_m^E(t)$ is the occupancy rate of the middle detector on the off-ramp at time t ; an occupancy threshold of 25% is used to determine whether the queue has reached the VDs or not (Liu *et al.*, 2007); D_h is the data collection frequency (e.g., 30 sec); and I_5 is a prespecified percentage and is set to 50% in this study.

Table 3.3 presents the procedures for determining the need for off-ramp control by examining if the off-ramp queue conditions reflect any of the following scenarios: 1) the off-ramp queue is expected to spill back to the freeway mainline in the next 5 min (step 1); 2) the off-ramp queue currently spills back (step 2); and 3) the off-ramp storage space is not well utilized (step 3).

After assessing the off-ramp queue conditions, the same logic (as shown in Table 3.4) will be applied to identify if the on-ramp queues under the adopted metering control will be in any of the following conditions: 1) having queue spillback in the next 5 min (step 1); 2) currently experiencing the queue spillbacks (step 2); and 3) exhibiting sufficient on-ramp storage space for ramp queues (step 3). Additionally, Table 3.5 summarizes the procedure for assessing the traffic flow rates over the local arterial's control boundaries. Specifically, when the detected entering flows to the control area are consistently higher than the predicted values, a traffic surge might be incurred, thus requiring a system-wide control.

Table 3.4 Procedure for assessing the on-ramp queue conditions

Step 1
If (at least I_6 percent of the initial metering cycles for ramp control over the next 5 min determined in Stage 2 $> \theta(Q^A)$) **and** ($S(\text{predicted flow rates on the freeway segment upstream of the on-ramp}) \geq 0$) **and** ($S(\text{predicted local boundary inflow rates}) \geq 0$)
then go to Step 4;
else go to Step 2;

Step 2
If ($S(\text{predicted arterial boundary inflow rates}) \geq 0$) **and** ($S(\text{detected occupancy rates of the upstream detector of the on-ramp}) \geq 0$) **and** ($\sigma_u^O(t - n_1 \cdot D_h) \geq 25\%, n_1 = 0 \text{ to } 1$) **and** ($\sigma_m^O(t - n_2 \cdot D_h) \geq 25\%, n_2 = 0 \text{ to } 5$)
then go to Step 4;
else go to Step 3;

Step 3
If ($S(\text{detected occupancy rates at the middle detector on the on-ramp}) < 0$) **and** ($S(\text{predicted arterial boundary inflow rate}) \leq 0$)
then go to Step 4;
else go to Step 5;

Step 4
 Stop **and** output "system-wide update needed."

Step 5
 Stop **and** output "system-wide update not needed."

Note: $\theta(Q^A)$ is the maximum ramp metering cycle length, corresponding to arterial traffic volume level Q^A , and should be prespecified in a way such that it can avoid on-ramp queue spillover in the next 5 min; $S(\cdot)$ presents the slope of the trend line of the target variable; $\sigma_u^O(t)$ denotes the occupancy rate of the upstream detector on the on-ramp at time t ; $\sigma_m^O(t)$ is the occupancy rate of the middle detector on the on-ramp at time t ; an occupancy threshold of 25% is used to determine whether the queue has reached the VDs or not (Liu *et al.*, 2007); D_h is the data collection frequency (e.g., 30 sec); and I_6 is a pre-selected percentage and is set to 50% in this study.

Table 3.5 Procedure for evaluating the arterial's boundary inflow rates

Step 1
If (at least I_7 percent of the differences between detected and predicted inflow rates over the past 5 min $> \gamma_7$) **and** ($S(\text{differences between the detected and predicted inflow rates}) \geq 0$)
then go to Step 2;
else go to Step 3;

Step 2
 Stop **and** output "system-wide update needed."

Step 3
 Stop **and** output "system-wide update not needed."

Note: $S(\cdot)$ presents the slope of the trend line of the target variable; I_7 is a pre-selected percentage and is set to 50% in this study; γ_7 is a pre-defined threshold and should be calibrated for each specific site based on the historical data.

Real-time control deactivation mechanism

The IRIC system is designed for mitigating recurrent traffic congestion during whole peak hours. To prevent the system from being terminated by temporal low demand, this study proposed the criteria and procedures used to determine if the system should deactivate its real-time operations and stay in the pre-timed mode, as shown in Table 3.6.

Table 3.6 Evaluation procedure for deactivation of real-time control

Step 1

At time t , for the past 10 min,

If (the computed ramp metering cycle lengths $= C_{o,min}$) **and** (detected freeway exiting flow rates $< \gamma_8$) **and** ($\sigma_u^E(k') < \gamma_9$) **and** ($\sigma_u^O(k') < \gamma_{10}$) **and** (detected arterial boundary inflow rates $< \gamma_{11}$) **and** ($S(\text{detected arterial boundary inflow rates}) \leq 0$)

then go to Step 2;

else go to Step 3;

Step 2

Stop **and** deactivate real-time control

Step 3

Stop **and** continue real-time control

Note: $C_{o,min}$ is a prespecified lower bound of the metering cycle length; $\sigma_u^E(k')$ and $\sigma_u^O(k')$ denote the occupancy rates of the upstream detectors on the off-ramp and on-ramp at time k' , respectively; $S(\cdot)$ presents the slope of the trend line of the target variable; and $\gamma_8, \gamma_9, \gamma_{10}$, and γ_{11} are pre-defined thresholds and should be calibrated for each specific site based on the historical data.

The system will make decisions to deactivate the real-time updates if any of the following criteria are met: 1) the computed ramp metering cycle lengths have been equal to the minimum value; 2) the detected freeway exiting flow rates have been less than a pre-defined threshold; 3) the detected occupancy rates by the upstream detector on the off-ramp and on-ramp are lower than a prespecified threshold; 4) the detected arterial boundary inflow rate has been lower than a pre-defined threshold; and 5) the trend of the detected arterial boundary inflow rates is non-increasing.

3.3 The optimization modules in the IRIC system

System-wide optimization module

The system-wide optimization module, which integrates the OQI (Chen et al., 2021a), LGB (Chen et al., 2021b), and AF-Ramp (Cheng and Chang, 2021) models, functions to maximize the total benefits of all motorists on the freeway segments and the local intersections based on real-time detected traffic conditions. This module should include the following set of formulations to realize all designed functions: 1) off-ramp constraints to ensure the absence of off-ramp queue spillback; 2) freeway throughput constraints to reflect its relation with the ramp metering cycle; 3) time-dependent on-ramp constraints to prevent on-ramp overflows; 4) intersection queue constraints for minimizing intersection queue spillovers; and 5) intersection flow conservation and signal timing-related constraints.

The computing flowchart of the optimization module is shown in Figure 3.6 and the key notations adopted in the formulations are listed in Table 3.7.

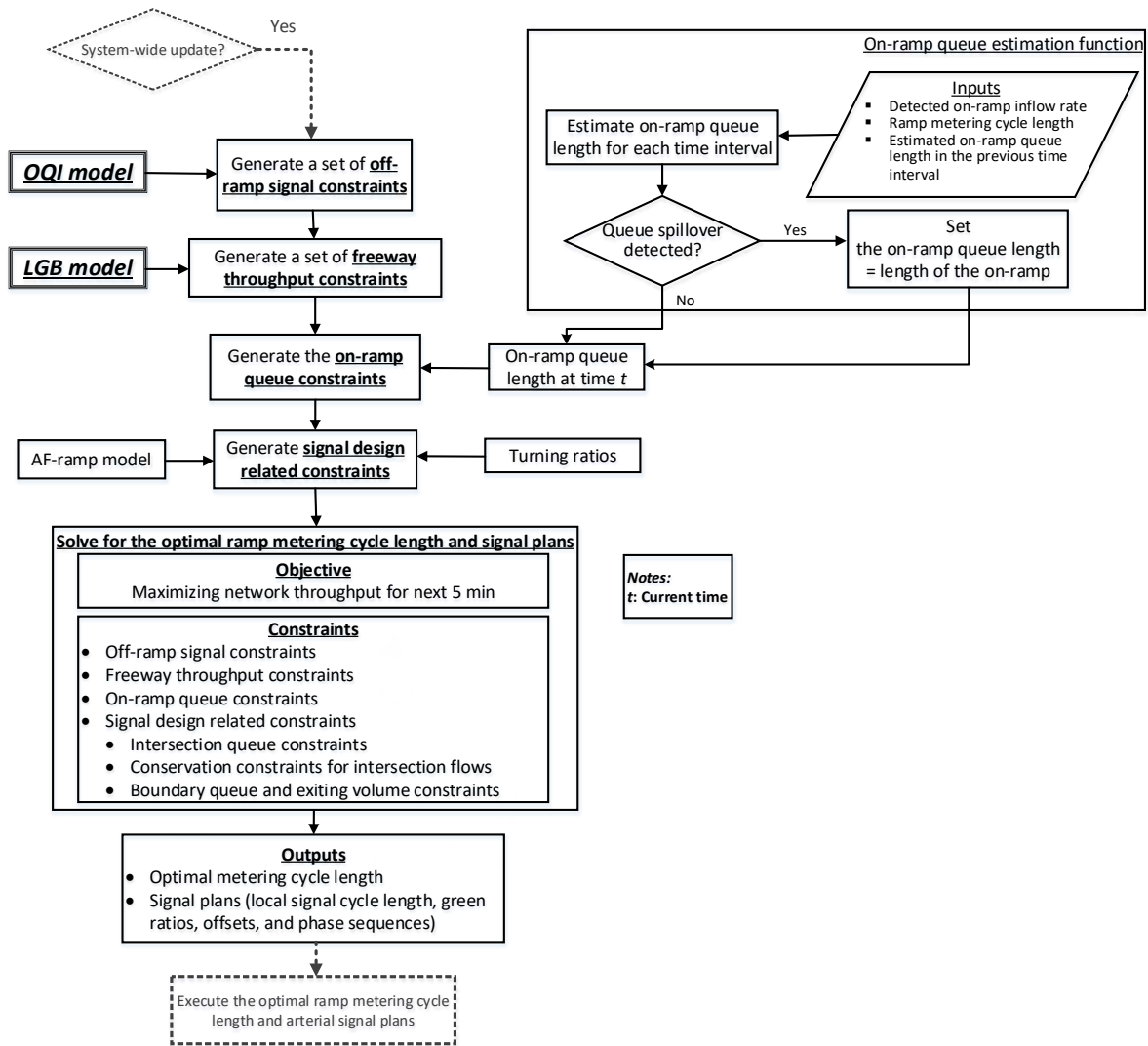


Figure 3.6 Flowchart of the system-wide optimization module

Table 3.7 Notation List

C_o	Metering cycle length (sec)
$C_{o,max}$	Maximal metering cycle length (sec)
$C_{o,min}$	Minimal metering cycle length (sec)
G_θ	Minimal green split which will not cause the off-ramp queue spillback under the given cycle length of θ seconds
H	Minimal space headway (m)
K	Elapsed intervals since the activation of the control system
L_o	On-ramp length (m)
R_{ϖ}	Number of queueing vehicles outside the target area due to the limited green time at intersection ϖ (veh)
V^A	Arterial throughput (vph)
V^F	Freeway throughput (vph)
V_μ^a	Actual volume for movement μ toward the on-ramp (vph)
Z	Entire control period (sec)
\dot{g}	Green split assigned to the off-ramp traffic
$l_e(k)$	On-ramp queue consisting of the arriving vehicles discharged per cycle from connected intersections (veh)
$l_p(k)$	On-ramp queue due to excessive on-ramp flows at the end of control interval k (veh)
r_o	Ramp metering rate
s_o	Saturation flow rate of the on-ramp (vph)
$q_o(k)$	Outflow rate of the on-ramp at control interval k (vph)
$\hat{q}_o(k)$	On-ramp entering flow rate at control interval k (vph)
$w_o(k)$	The number of vehicles in the on-ramp queue at the end of control interval k
Δk	Period of one control interval for arterial signals (sec) (e.g., 300 sec)
Ω	Set of intersection movements heading to the on-ramp
β_1, β_2	Weighting factors
θ_{max}	Upper bound of local signals' cycle length (sec)
θ_{min}	Lower bound of local signals' cycle length (sec)
ξ	Reciprocal of the cycle length at the arterial intersections (1/sec)

Off-ramp signal constraints

To avoid off-ramp queue spillback, the system-wide optimization module is embedded with a set of constraints on the minimum green split allocated to the off-ramp flows, denoted as G_θ , for each given cycle length, θ , as shown in Equation 3.5. Such lower bounds are determined based on the results produced from the OQI model (Chen et al., 2021a) and will ensure the absence of off-ramp queue spillover to the freeway mainline.

$$\dot{g} \geq G_\theta, \text{ if } \frac{1}{\xi} = \theta \ (\forall \theta \text{ between } \theta_{min} \text{ and } \theta_{max}) \quad (3.5)$$

Freeway throughput constraints

Given the inputs of flow rates at the ramp and on its upstream freeway segment, the LGB model (Chen et al., 2021b) will function to produce the estimated freeway throughput over the control area. Considering the non-convexity of the LGB model (Chen et al., 2021b), however,

integrating all its equations into the mathematical programming in the optimization module may not yield the solution sufficiently efficient for real-time needs. Hence, this section has constructed a series of constraints, as shown in Equation 3.6, reflecting the relation between the given ramp cycle length, ω , and the corresponding freeway throughput obtained by the LGB model (Chen et al., 2021b), denoted as \widehat{V}_ω .

$$V^F = \widehat{V}_\omega, \text{ if } C_o = \omega (\forall \omega \text{ between } C_{o,min} \text{ and } C_{o,max}) \quad (3.6)$$

Note that a constraint will be generated for each possible value of C_o so that the computation of the LGB model (Chen et al., 2021b) will be conducted in advance and not be involved in the optimization process.

On-ramp queue constraints

The on-ramp queue constraints are developed to ensure that the on-ramp queue would not exceed the on-ramp length due to ramp metering during the whole control period. The ramp queue typically consists of two components: 1) the residual queues due to the difference between the on-ramp's entering and exiting flows; and 2) the arriving vehicles discharged per cycle from those intersections within the control zone. One can formulate Equation 3.7 to calculate the former at the end of the next control interval and let the latter be expressed by Equation 3.8.

$$l_p(k+1) = \max \left(w_o(k) + \left(\sum_{\mu \in \Omega} V_\mu^a - s_o r_o \right) \cdot \frac{\Delta k}{3600}, 0 \right) \quad (3.7)$$

$$l_e(k+1) = \sum_{\mu \in \Omega} V_\mu^a / 3600 \xi \quad (3.8)$$

$$w_o(k) = \max \left(\min \left(w_o(k-1) + \frac{\Delta k}{3600} * (\hat{q}_o(k-1) - q_o(k-1)), \frac{L_o}{H} \right), 0 \right) \quad (3.9)$$

where $l_p(k+1)$ represents the on-ramp queue length due to excessive on-ramp flows at the end of time interval $(k+1)$, to be updated by the on-ramp queue estimation function when an on-ramp queue spillover is not detected, as shown in Equation 3.9. If a queue spillover is detected, $w_o(k)$ will be set to (L_o/H) . Note that such queue length may decrease if, during the next control interval, the on-ramp arriving flow rate is lower than the metering rate. The right-hand side of Equation 3.8 sums up all traffic flows entering the on-ramp during one signal cycle from the surface intersections.

To ensure that the on-ramp queue length does not increase rapidly at the start of the peak period, the allowed upper bound for the on-ramp queue length should be proportional to the ratio of the elapsed time over the total period, as expressed in Eq. (3.10).

$$l_p(k) \leq \min \left(\left(\frac{k}{Z} (L_o/H - l_e(k)), (L_o/H - l_e(k)) \right) \right) \quad (3.10)$$

In Equation 3.10, $(L_o/H - l_e(k))$ is used to calculate the available space for the vehicle queues caused by excessive on-ramp flows.

With the objective function of maximizing the total throughput of the network, the completely system-wide optimization module is set as follows:

$$\text{Max } V^F + \beta_1 V^A - \beta_2 \sum_{\omega} R_{\omega}$$

s.t.

Off-ramp signal constraint: Equation 3.5

Freeway throughput constraint: **Equation 3.6**

On-ramp queue constraints: **Equations 3.7, 3.8, and 3.10**

Signal design-related constraints (Cheng and Chang, 2021)

Ramp metering optimization module

The flowchart of the ramp metering optimization module is shown in Figure 3.7. When re-optimizing the ramp control alone is justified, its primary control objective is to maximize the freeway throughput. Following the logic of the system-wide optimization module, the LGB model (Chen et al., 2021b) will be adopted to predict the freeway throughputs under the set of candidate metering cycle lengths (i.e., between maximal and minimal metering cycle lengths), as expressed with the right-hand side of Equation 3.6. The complete ramp metering optimization module is shown below,

Max V^F

s.t.

Freeway throughput constraint: **Equation 3.6**

Where, V^F is the freeway throughput.

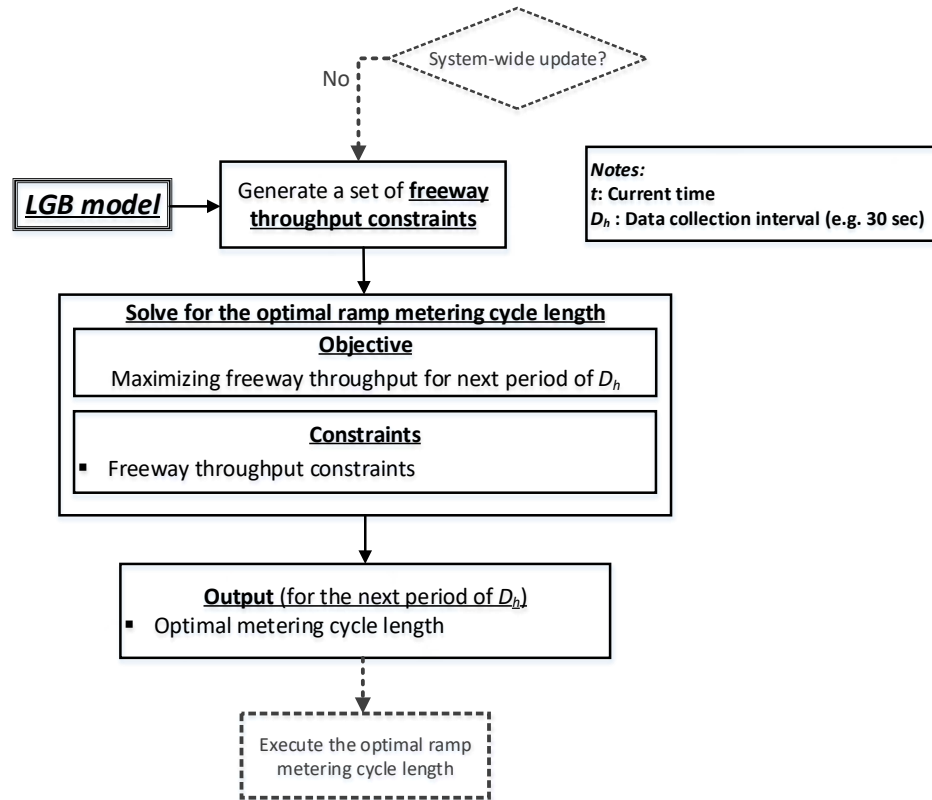


Figure 3.7 Flowchart of the ramp metering optimization module

3.4 Case Study

The proposed IRIC system has integrated three major functions: 1) an off-ramp signal control system to address the off-ramp queue spillovers' impacts on freeway mainline segments, 2) an on-ramp metering control system to ensure that the on-ramp queue does not exceed the ramp length, and 3) a local signal control system to simultaneously prevent gridlocks on arterial links and

provide progressions to local and freeway exiting traffic. Ideally, one may select a comparable integrated real-time control model with all such key functions capabilities as the benchmark model for the case studies. However, as far as the authors recognize, such an integrated control strategy with comprehensive functions for all traffic flows within the interchange area remains lacking in the literature. With regard to off-ramp signal control, a few studies (Li et al., 2009; Lim et al., 2011; Zhao and Liu, 2016; Yang et al., 2014; Yang et al., 2018; Chang et al., 2020; Chen et al., 2021a) has involved similar functions as in the proposed system, but mostly for pre-timed control. In terms of on-ramp metering control, limited studies (Tian et al., 2005; Tian, 2007; Chang et al., 2020; Cheng and Chang, 2021) took advantage of coordinating local signals with ramp meters to balance freeway and local traffic conditions. Again, these studies are mainly for pre-timed strategies.

Since this study evolved from the fixed-time AF-ramp system (Cheng and Chang, 2021), adopting AF-ramp and its enhancement with off-ramp considerations as the benchmark strategy can reveal the advantages of the proposed IRIC system regarding the real-time control functions and optimization modules. Noticeably, several studies evaluated the performance of their real-time control strategies by comparing them with their corresponding pre-timed strategies (Dai et al., 2011; Pranevičius and Kraujalis, 2012; Wang et al., 2012; Cui et al., 2014). To develop a convincing benchmark model for a fair comparison, the OQI model (Chen et al. 2021a) has been integrated with the AF-ramp to mitigate the impact of both on-ramp and off-ramp queue spillovers in the design of the off-ramp signal. The measures of effectiveness (MOE) for performance evaluation include speeds on freeway segments upstream of the off-ramp and on-ramp, freeway and arterial delays, maximal ramp and intersection queue lengths, average delays, and total throughputs.

Case study design

Figure 3.8 shows the geometric features associated with Exit 36 of I-495 in Maryland and its neighboring intersections on Old Georgetown Road with the locations of the required vehicle detectors (VDs) in the proposed IRIC system. The initial phase design is shown in Figure 3.8, and the phase sequences and green splits are optimized by the proposed system. The proposed system will be evaluated with two volume scenarios with time-varying flow rates. The turning ratios and average flow rates in each scenario are shown in Tables 3.8 and 3.9, respectively, with Scenario 2 reflecting a higher freeway mainline volume. The off-ramp ratio is set to be 0.16 in both scenarios.











Phase ID Intersection	1	2	3	4
1				
2				
3				

Figure 3.8 The phase design for all intersections

Table 3.8 The turning ratios for all intersections

Intersection	NB			SB			EB			WB		
	L	T	R	L	T	R	L	T	R	L	T	R
1	0.01	0.98	0.01	0.04	0.95	0.01	0.92	0.04	0.04	0.39	0.01	0.6
2	-	0.7	0.3	0.25	0.75	-	0.9	0	0.1	-	-	-
3	0.14	0.86	-	-	0.8	0.2	-	-	-	0.5	0	0.5

Note: NB = Northbound, SB = Southbound, EB = Eastbound, WB = Westbound, L = Left-turn, T = Through, R = Right-turn

Table 3.9 The distributions of flow rates at each key location in two experimental scenarios

Time (sec.)	Scenario	A (freeway mainline; 3 lanes)	B (1 lane)	C (3 lanes)	D (2 lanes)	E (2 lanes)	F (3 lanes)
		0 - 600	1	3300	250	600	500
	2	3465					
600 - 1500	1	5500	250	1100	500	250	1200
	2	5775					
1500 - 2400	1	4200	250	800	500	250	1200
	2	4410					
2400 - 3000	1	5500	250	1100	500	250	1200
	2	5775					
3000 - 3600	1	3800	250	600	500	250	800
	2	3990					

The IRIC system was built on VISSIM 10, a stochastic microsimulation software by PTV AG (2018), for evaluation. The IRIC system, incorporating the functions of the OQI and LGB models, is coded with VB.NET and communicates with VISSIM via the COM interface. The optimization modules are solved with Gurobi 9 (Gurobi Optimization, 2020) on a Windows 10 desktop with an Intel Core i7-9700 processor and 16 GB RAM. The computation times of the system-wide optimization module and ramp metering optimization module are less than 10 seconds and 1 second, respectively. The resulting MOEs, including delay, throughput, and queue lengths for performance comparison, are directly generated from the simulation outputs of VISSIM. Five random seeded simulation runs were performed in VISSIM and the results are averaged.

Evaluation results

The section presents the performance comparisons between the IRIC system and the pre-timed model. The signal plans optimized by the based pre-timed control model, including green splits, offsets, phase sequences, and cycle time, are shown in Figure 3.9. Note that the two fixed-timed plans have been generated for a more rigorous comparison, where Plan A is optimized with the average flow rates during the control period of 600 to 3000 seconds, and Plan B has been produced with the maximum flow rates (i.e., those between 600 and 1500 seconds.). The metering

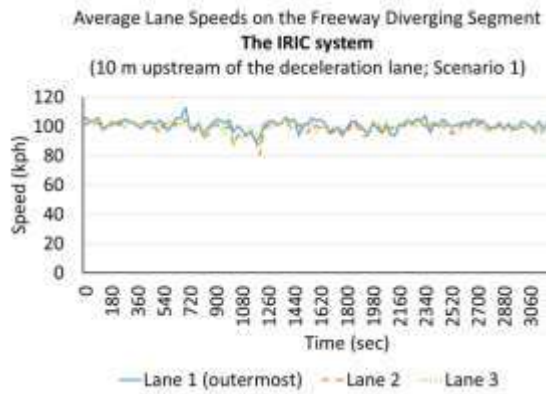
rates are 0.34 and 0.36 for plans A and B, respectively. The metering control in the case study will be operated under 2-cars per green interval.

Fixed-time signal plan	Intersection	Phase ID			
		1	2	3	4
A	1 (0)	41s ↓↑	14s ↘	19s ⇒⇒	16s ⇒⇒
	2 (2)	27s ↓↑	30s ↓↘	33s ⇒⇒	
	3 (47)	23s ↓↑	53s ↗↑	14s ←⇒	
B	1 (0)	32s ↓↑	23s ↘	19s ⇒⇒	16s ⇒⇒
	2 (0)	22s ↓↘	29s ↓↑	39s ⇒⇒	
	3 (8)	26s ↓↑	22s ↗↑	42s ←⇒	

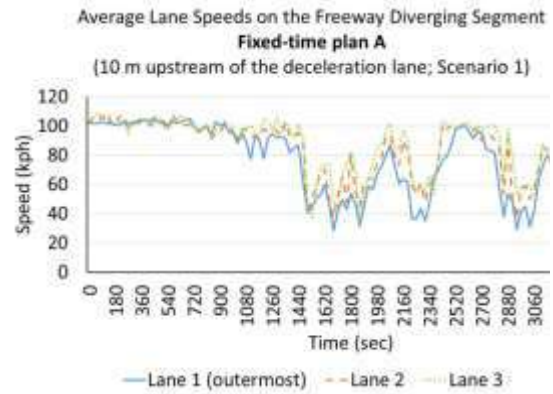
Figure 3.9 The fixed-time signal plans

Figure 3.10 shows the average lane speeds on the freeway segment upstream of the off-ramp under the IRIC system and fixed-time controls in Scenario 1. The results illustrate that the IRIC system has allocated adequate green time at the off-ramp intersection to adapt to volume fluctuation. As a result, the lane speeds on the freeway segments with the real-time interchange control under this scenario are all above 80 kph (see Figure 3.10 (a)).

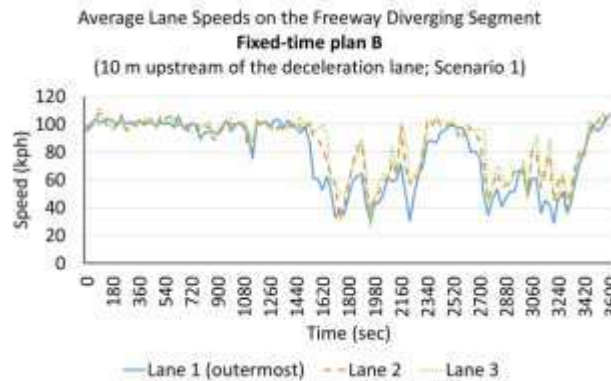
Conceivably, with the fixed-time control, the system may not respond in time to the volume fluctuation, even though the control plan is optimized with the highest flow rate during the control period (i.e., plan B). This is evident in the simulation results that show lane speeds on the freeway segment are less than 40 kph under both fixed-time plans A and B (see Figure 3.10 (b) and Figure 3.10 (c)).



(a) IRIC system



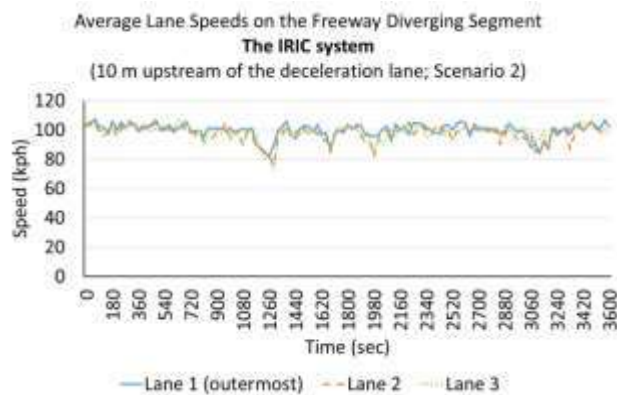
(b) Fixed-time plan A



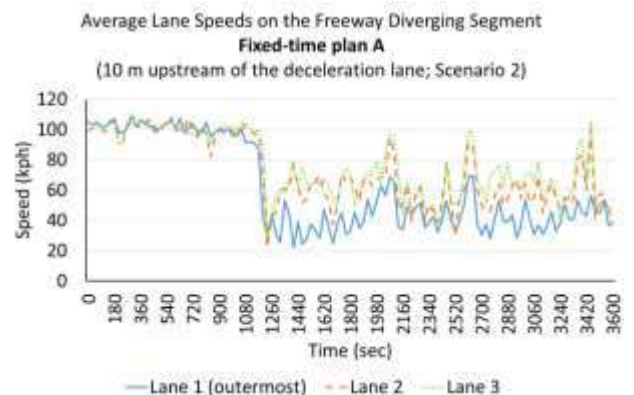
(c) Fixed-time plan B

Figure 3.10 Average lane speeds of the control strategies on the freeway diverging segment under Scenario 1. (a) IRIC system; (b) Fixed-time plan A; (c) Fixed-time plan B

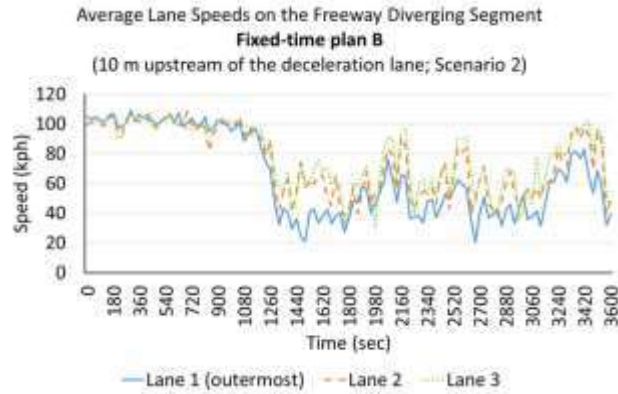
Note that for the scenario of higher exiting volume (i.e., Scenario 2), the IRIC system can still well adjust the off-ramp signal plan to prevent the off-ramp queue from spilling back to the freeway mainline and avoid traffic breakdown, as shown in Figure 3.11 (a). Under such a scenario, all lane speeds on the freeway segment remain above 70 kph under the IRIC control—significantly better than the resulting averages of about 20 kph if with the off-line fixed-time control operations (see Figure 3.11 (b) and Figure 3.11 (c)).



(a) IRIC system



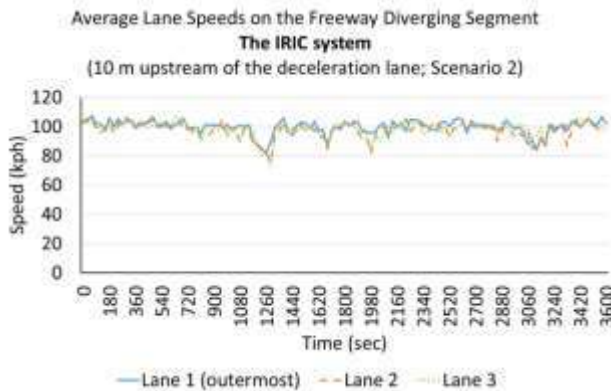
(b) Fixed-time plan A



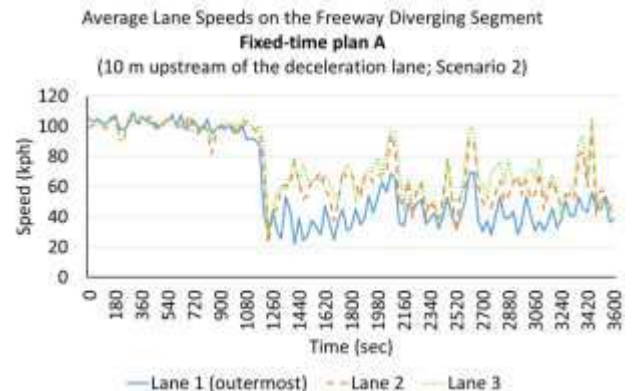
(c) Fixed-time plan B

Figure 3.11 Average lane speeds of the control strategies on the freeway diverging segment under Scenario 2. (a) IRIC system; (b) Fixed-time plan A; (c) Fixed-time plan B

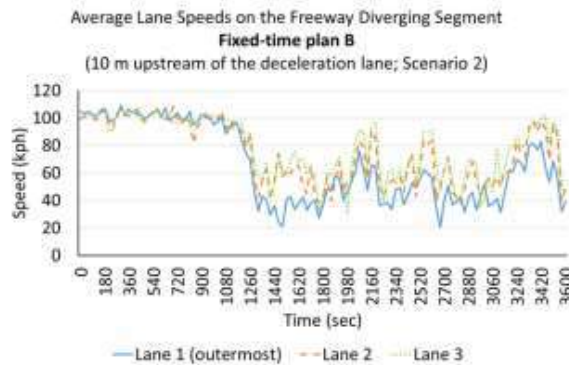
With respect to the freeway segment receiving on-ramp flows, its lane speeds are all above 50 kph under both the IRIC system and fixed-time controls in Scenarios 1 and 2, as shown in Figure 3.12 and Figure 3.13, respectively. The fixed time controls, however, result in much higher traffic delays for on-ramp vehicles (see Figure 3.14 (a) and Figure 3.14 (b)). More specifically, under Scenario 1, the total on-ramp vehicle delay under real-time control is 4.0 veh-hours, much less than 31.9 and 13.3 veh-hours, respectively, under fixed-time plans A and B.



(a) IRIC system

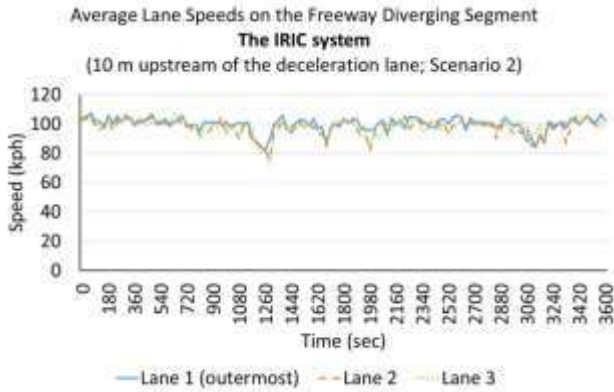


(b) Fixed-time plan A

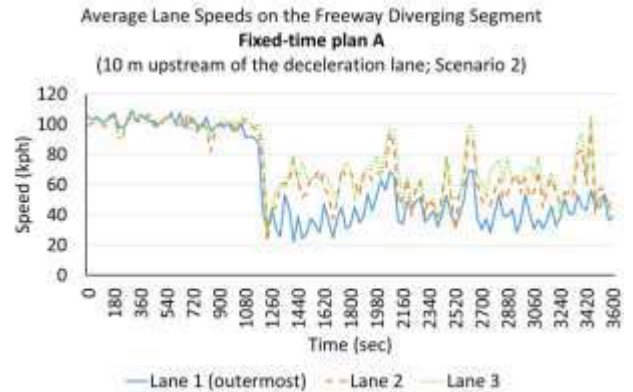


(c) Fixed-time plan B

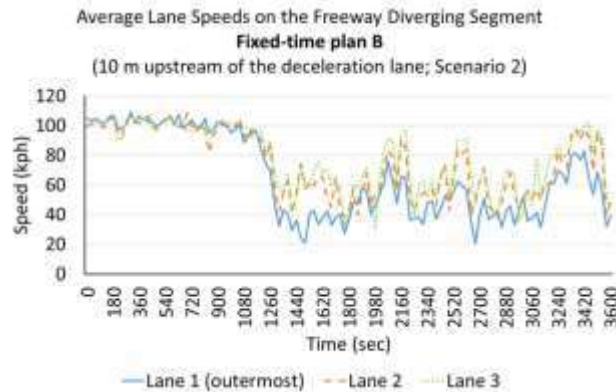
Figure 3.12 Average lane speeds of the control strategies on the freeway segment upstream of the on-ramp under Scenario 1. (a) IRIC system; (b) Fixed-time plan A; (c) Fixed-time plan B



(d) IRIC system



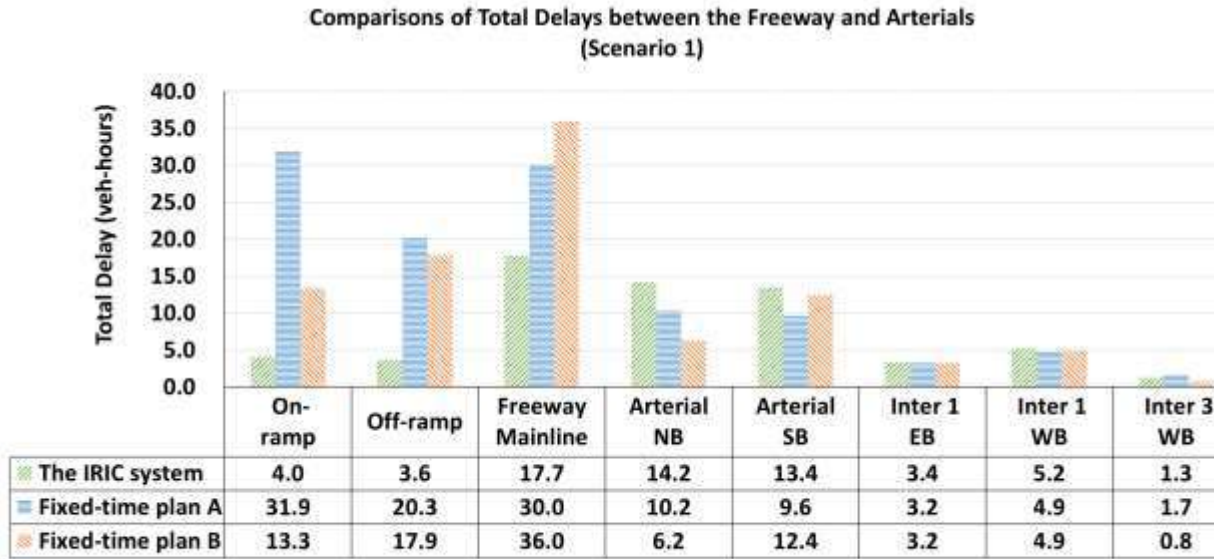
(e) Fixed-time plan A



(f) Fixed-time plan B

Figure 3.13 Average lane speeds of the control strategies on the freeway segment upstream of the on-ramp under Scenario 2. (a) IRIC system; (b) Fixed-time plan A; (c) Fixed-time plan B

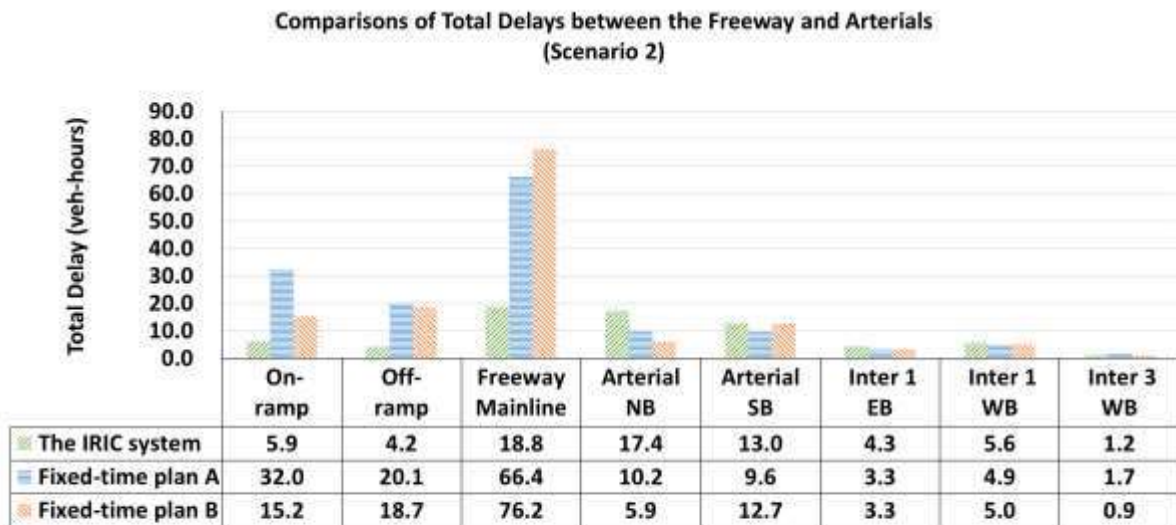
In addition, since the IRIC system can flexibly allocate sufficient green times to the exiting flows under the scenarios of volume fluctuation, its resulting delays at the off-ramp connected segment and on the freeway mainline delays are much lower than those under the fixed-time controls, as shown in Figure 3.14 (a) and Figure 3.14 (b), where the freeway mainline delays under the IRIC system, signal plan A, and signal plan B are 17.7, 30.0, and 36.0 veh-hours, respectively, under Scenario 1.



Arterial, Ramp, and Freeway Mainline

Unit: veh-hours

(a) Scenario 1



Arterial, Ramp, and Freeway Mainline

Unit: veh-hours

(b) Scenario 2

Figure 3.14 Total delays between the freeway and arterials. (a) Scenario 1; (b) Scenario 2

As expected, the advantage of the real-time control is more evident when the volume increases (i.e., Scenario 2). The freeway mainline delays in Scenario 2 increase from 30.0 to 66.4 veh-hours under the fixed-time plan A, and from 36.0 to 76.2 veh-hours under Plan B. By contrast, the freeway mainline delays with the IRIC system are consistently below 20 veh-hours in both scenarios (see Figure 3.14 (a) and Figure 3.14 (b)).

Additionally, the IRIC system also outperforms the fixed-time controls with respect to the average delays of the whole network (see Table 3.10). For example, under Scenario 2, compared to fixed-time plans A and B, the IRIC system achieves the improvements of 57.87% (43.9 vs. 104.2 sec/veh) and 47.86% (43.9 vs. 84.2 sec/veh), respectively. Moreover, the performance of real-time control is more stable under high volume scenario. As is notable from the results in Table 3.10, when the freeway volume increases by 5% (i.e., from Scenario 1 to Scenario 2), the average delay under the IRIC system increases by about 10.86% (from 39.6 sec/veh in Scenario 1 to 43.9 sec/veh in Scenario 2), far less than the 25.54% and 15.98%, under the fixed-time plans A and B, respectively. The box and whisker plot depicting the average delay results of all simulations is shown in Figure 3.15. One can see that average delays under the IRIC system are much lower than those under signal plans A and B in all simulation runs. This further supports that the performance of the proposed control system is stable.

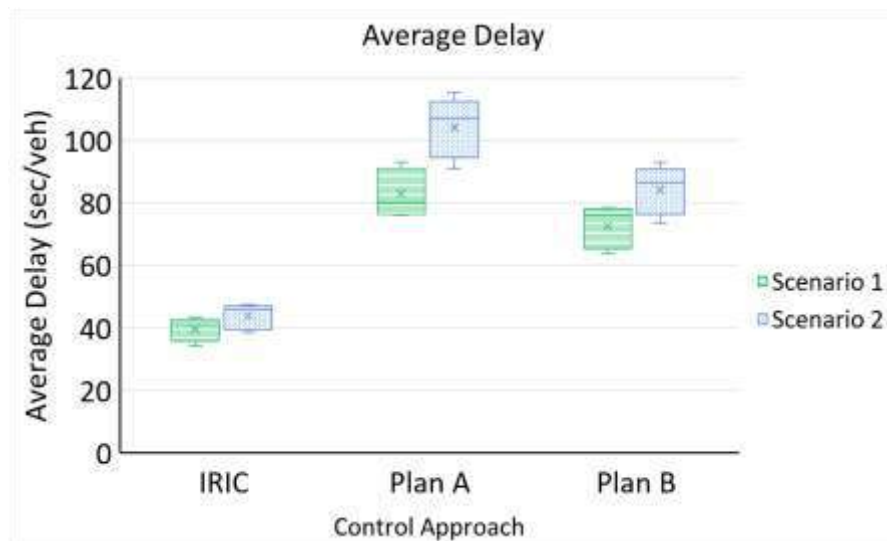


Figure 3.15 The box and whisker plot of resulting average delays

Table 3.10 Average delays under Scenarios 1 and 2

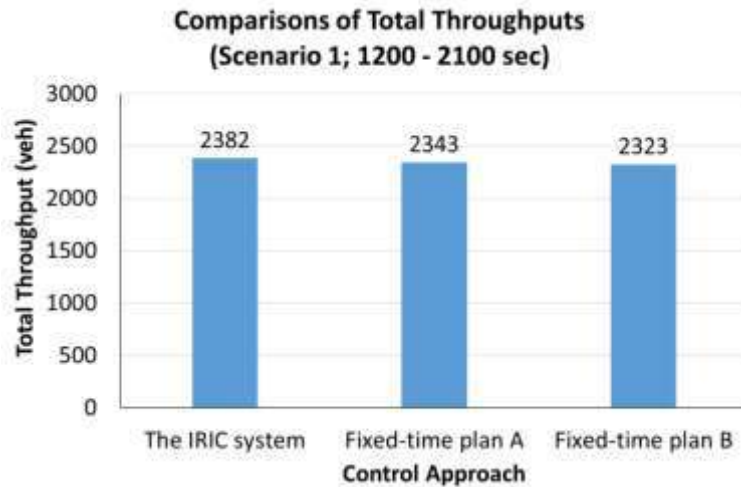
Scenario	IRIC system (sec/veh)	Fixed-time plan A (sec/veh)	Fixed-time plan B (sec/veh)	Improvement (%)	
				Compared to plan A ²	Compared to plan B ²
1	39.6	83.0	72.6	52.29%	45.45%
2	43.9	104.2	84.2	57.87%	47.86%
Increment¹ (%)	10.86%	25.54%	15.98%		

¹ Increment = (average delay of the control approach under Scenario 2 - average delay of the control approach under Scenario 1)/(average delay of the control approach under Scenario 1)*100%

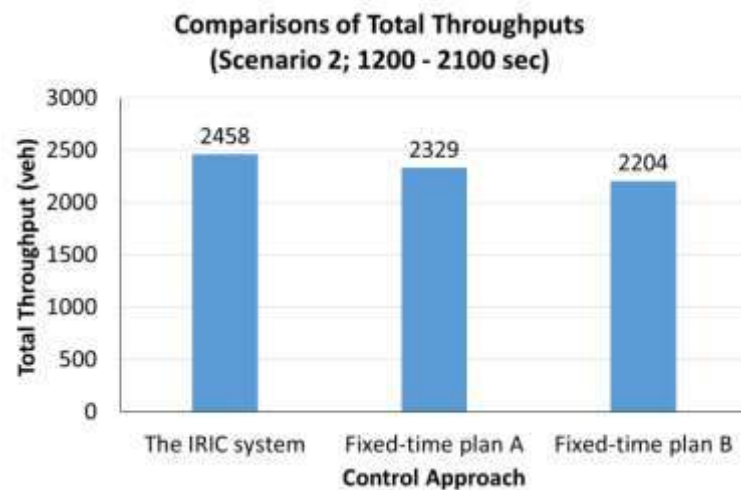
² Improvement = (average delay of the fixed-time control - average delay of the IRIC system)/(average delay of the fixed-time control)*100%

The total throughputs for Scenarios 1 and 2 during the peak period are shown in Figure 3.16 (a) and Figure 3.16 (b), respectively. The total throughputs of the IRIC system under Scenario 1 are 1.66% (2382 vs. 2343 vehs) and 2.54% (2382 vs. 2323 vehs), slightly higher than those from fixed-time plans A and B, respectively. The advantage of the IRIC system on total throughput becomes more pronounced with an increase in traffic volume, as reflected in its improvement of

5.54% (2458 vs. 2329 vehs) and 11.52% (2458 vs. 2204 vehs) over fixed-time plans A and B, respectively, in Scenario 2.



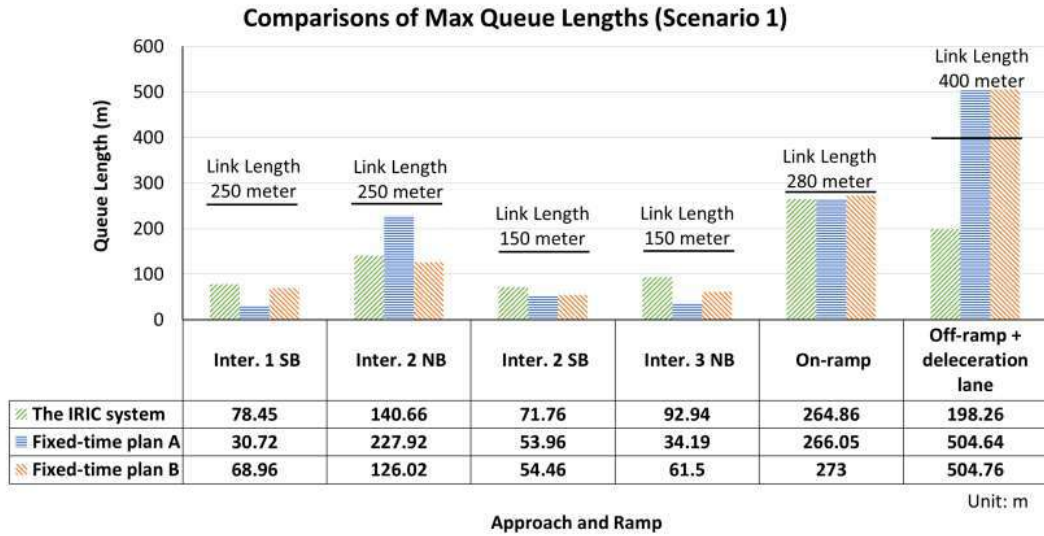
(a) Scenario 1



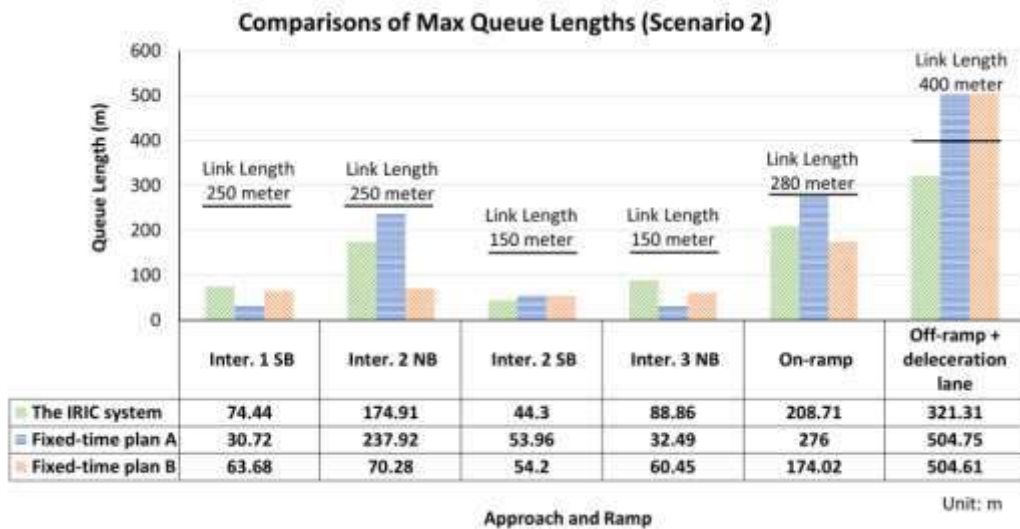
(b) Scenario 2

Figure 3.16 Total throughputs. (a) Scenario 1; (b) Scenario 2

Figure 3.17 (a) and Figure 3.17 (b) show that the IRIC system can efficiently avoid queue spillbacks on the arterial links and freeway ramps in the control area in Scenarios 1 and 2. Under such a real-time control system, the maximal queues on all arterial links are shorter than their lengths in both Scenarios 1 and 2. In contrast, the off-ramp queue lengths under the fixed-time controls are likely to spill back onto the freeway mainline (see Figure 3.17 (a) and Figure 3.17 (b)).



(a) Scenario 1



(b) Scenario 2

Figure 3.17 Maximal queue lengths on the links. (a) Scenario 1; (b) Scenario 2

3.5 Discussion

To contend with recurrent traffic congestion in a freeway's interchange area, including freeway mainline, on/off-ramps, and nearby local arterials, this study has developed an Integrated Rreal-time Interchange Control (IRIC) system that can concurrently maximize the system throughput of both freeway and local arterial users. Such a system can serve as a flexible tool for operators to concurrently optimize both ramp metering and local signal controls under different traffic and geometric conditions, or to execute each independently.

The proposed system is capable of selecting a proper control strategy with its traffic monitoring function, choosing between system-wide optimization for the entire control area and ramp-only control based on the real-time detected traffic volume obtained from both the freeway

mainline and the arterial entering links. The embedded system-wide optimization module integrates the OQI and LGB models to optimize the ramp metering cycle length and local signal plans, which can prevent both on-ramp spillback to the surface street and off-ramp queue spillover to the freeway mainline. For the needs of real-time operations, a series of constraints on the off-ramp intersection signal and ramp metering cycle length are produced in advance by the OQI and LGB models. This is done so that the complex optimization problem can be formulated as mixed-integer linear programming with desirable computational efficiency.

The results from experiments evidenced the benefits of the system's real-time mode over its off-line operations, especially with respect to preventing off-ramp queue spillback. It also proved effective in utilizing the capacity of the freeway merging segment to reduce on-ramp waiting time and the likelihood of queue spillback, both of which are key factors contributing to the interchange congestion.

Despite the progress made in this study on real-time interchange control, much remains to be done. The IRIC system is applicable to an interchange area where the off-ramp is at the upstream of its on-ramp and there are no exiting and entering flow streams between these ramps. More experimental tests will need to be conducted to validate the performance of an IRIC system applied to an interchange area with weaving behaviors between ramps, such as a cloverleaf interchange without collector-distributor (C-D) roads. Also, although the IRIC system possesses the capability of reacting responsively to real-time demand variations, it is designed to mitigate recurrent traffic congestion. How to enhance the IRIC system to contend with non-recurrent traffic congestion is another interesting and meaningful research direction. In addition, some of the other vital subjects to be further investigated include: 1) Extending the control scope to multiple interchanges and surrounding arterials along the freeway corridor under both recurrent and non-recurrent congested scenarios; 2) Incorporating demand management strategies with an integrated corridor control system; 3) Enhancing real-time control under the connected and autonomous vehicle (CAV) environment; and 4) Investigating how irregular the traffic volume must be for the proposed system to start demonstrating its effectiveness.

Chapter 4: Future Research Extension

4.1 Conclusions

This research has produced an arterial friendly ramp metering control system for real-time operations and an extension to cover the entire interchange, including off-ramp signal controls. The results of performance evaluation with extensive simulation scenarios have demonstrated that the developed system can indeed optimize ramp metering flows with minimal impacts on the neighboring local traffic. Based on the commonly used MOEs, both developed systems seem to clearly outperform state-of-the-art models designed to address the same recurrent congestion on freeway segments and queue spillback from local ramps to neighboring arterials. By extending the control area to nearby off-ramps, the benefits from coordinated freeway ramp controls with local traffic signals can be extended to the entire freeway interchange, which is often the primary bottleneck in a commuting corridor.

To ensure the proposed system's effectiveness in addressing complex, local-specific traffic patterns, it is essential to conduct a rigorous and extensive field evaluation with respect to the system's key model parameters and embedded assumptions. The coordinated relationship between the system's three primary models, from estimating the freeway's remaining capacity for ramp flows to the optimization of ramp metering rate and intersection signal plans, can also be assessed with field data. Most importantly, after all key parameters of the AF-Ramp system have been calibrated, one can observe the system's performance from its field operations with respect to its three key control objectives: (1) maximizing the freeway's throughput under the optimized ramp metering rate; (2) preventing ramp queues from spilling over to its neighboring arterial; and (3) mitigating the potential mutual impedance between the arterial's through traffic and its turning-flows to the ramp with the coordinated signal timings, variable phase sequences, and progression offsets.

Note that despite the promising performance observed from extensive simulated traffic scenarios, any new control technology or systems must go through extensive tests using real-world data and feedback from target deployment locations. This ensures that any necessary enhancements or refinements can be implemented prior to field deployment. Only after achieving expected performance from field evaluation can the AF-ramp transition from academic work to a well-calibrated, deployable system on Maryland's highway networks.

4.2 Further evaluation with field data

With a focus on field performance, future extensions for this study shall include: (1) conducting the field evaluation and refinement of the **AF-Ramp** system, and (2) streamlining the system's control configuration and its parameter updating procedures for field implementation.

It is expected that this study, after completing all essential evaluation and refinement tasks, will convert the mathematical formulations of all three models into three user-friendly computer programs that can be used independently for their own target applications, or integrated in the AF-Ramp system's operating structure for executing the freeway-arterial coordinated network controls.

In general, a rigorous field evaluation plan shall contain at least the following tasks:

Task-1: Identification of candidate sites and data items for field evaluation

To have sufficient information for the field evaluation, collected traffic data must include: (1) the freeway segment's speed by lane before and after merges from the ramp flows during congested peak periods; (2) average ramp volume, speed, and queue length (if any) during the congested peak periods; (3) signal plan for each neighboring intersection, including the cycle length, phase sequence, phase duration, and offset; and (4) performance of the current signal plan, including the average and maximum queue length for each intersection movement, and the average delay per vehicle at each local intersection.

Task-2: Design of the data collection plan

To design a comprehensive data collection plan for field evaluation, the critical information to be considered shall include: (1) *time interval* for each collected traffic data; (2) *the sample size* of the field data collected for parameter calibration, model performance evaluation, and model stability analysis; and (3) *the precision level* of traffic characteristic variables (e.g., speed data by lane per minute, intersection queue per lane and per cycle) collected for each model's calibration and performance evaluation.

Task-3: Calibration of key model parameters from field data with a customized algorithm

As with all traffic control models used in practice, one needs to calibrate key parameters in the AF-Ramp system prior to its field evaluation or implementation. This is to ensure that all embedded prediction and control algorithms have sufficiently reflected the unique behavioral characteristics of the local driving populations, as well as the geometric and operational constraints associated with the target freeway segment and intersections within the control boundaries.

Task-4: Design of the plan for evaluating the AF-Ramp system's performance with field data

Since each model in the AF-Ramp system's operations has its own role, the evaluation plan should be so designed to best fit each model's features and its role in the overall system's control environment. Hence, the measures of effectiveness (MOEs) and the method for performance and reliability analysis should include: (1) monitoring and prediction of the target freeway's traffic conditions; (2) producing the optimal metering rate and coordinated local signal plans; and (3) assessing progression bandwidth for the arterial's through and turning flows.

Task-5: Conducting the System demonstration, evaluation, and refinements.

The core of the final evaluation task shall consist of the following research analyses: (1) *off-line pre-deployment simulation of the system's effectiveness* regarding interactions between its key models; (2) *on-line demonstration of the AF-Ramp system* with deployed traffic sensors, ramp signals, and intersections within the ramp-impact area; and (3) *System refinement based on the results from the field demonstration*. Major efforts of this task shall be devoted to (1) identifying any necessary improvement to ensure the system's robustness with respect to potential traffic volume surge or sensor malfunction; (2) streamlining the system's operating process to minimize any potential human errors; and (3) assessing the quality and reliability of the control hardware and sensors used in the on-line operations, and providing some guidelines for future field system deployment.

REFERENCES

1. Agarwal, S., Kachroo, P., Contreras, S., and Sastry, S. (2015). Feedback-coordinated ramp control of consecutive on-ramps using distributed modeling and Godunov-based satisfiable allocation. *IEEE Transactions on Intelligent Transportation Systems*, 16 (5), 2384-2392.
2. Achillides, C., & Bullock, D. (2004). Performance Metrics for Freeway Sensor. Joint Transportation Research Program, 164.
3. Carlson, R. C., Papamichail, I., and Papageorgiou, M. (2014). Integrated feedback ramp metering and mainstream traffic flow control on motorways using variable speed limits. *Transportation Research Part C: Emerging Technologies*, 46, 209-221.
4. Carlson, R. C., Papamichail, I., Papageorgiou, M., and Messmer, A. (2010a). Optimal motorway traffic flow control involving variable speed limits and ramp metering. *Transportation Science*, 44 (2), 238-253.
5. Carlson, R. C., Papamichail, I., Papageorgiou, M., and Messmer, A. (2010b). Optimal mainstream traffic flow control of large-scale motorway networks. *Transportation Research Part C: Emerging Technologies*, 18(2), 193-212.
6. Chang, G. L., Cheng, Y., Chen, Y. Y., & Chen, Y. H. (2020). *Integration of Ramp Metering and Off-Ramp Progression* (No. MD-20-SHA/UM/5- 14). Maryland. Dept. of Transportation.
7. Chen, Y. Y. (2021). *An Integrated Real-Time Interchange Control System* (Doctoral dissertation), University of Maryland, College Park.
8. Chen, Y. Y., Chen, Y. H., and Chang, G. L. (2021a). Optimizing the integrated off-ramp signal control to prevent queue spillback to the freeway mainline. *Transportation Research Part C: Emerging Technologies*, 128, 103220.
9. Chen, Y. Y., Cheng, Y., and Chang, G. L. (2021b). Lane Group-Based Traffic Model for Assessing On-Ramp Traffic Impact. *Journal of Transportation Engineering, Part A: Systems*, 147(2), 04020152.
10. Cheng, Yao, and Chang, Gang-Len (2021). An arterial-friendly local ramp metering control strategy. *Transportation Research Record: Journal of the Transportation Research Board*.
11. Chow, A. H., and Li, Y. (2014). Robust optimization of dynamic motorway traffic via ramp metering. *IEEE Transactions on Intelligent Transportation Systems*, 15 (3), 1374-1380.
12. Cui, C., Cui, J., & Lee, H. (2014). Real-time stochastic optimal control for traffic signals of multiple intersections. *Artificial Life and Robotics*, 19(2), 142-149.
13. Dai, Y., Hu, J., Zhao, D., & Zhu, F. (2011, October). Neural network based online traffic signal controller design with reinforcement training. In 2011 14th International IEEE Conference on Intelligent Transportation Systems (ITSC) (pp. 1045-1050). IEEE.
14. Frejo, J. R. D., and Camacho, E. F. (2012). Global versus local MPC algorithms in freeway traffic control with ramp metering and variable speed limits. *IEEE Transactions on Intelligent Transportation Systems*, 13 (4), 1556-1565.
15. Frejo, J. R. D., and De Schutter, B. (2018). Feed-Forward ALINEA: A ramp metering control algorithm for nearby and distant bottlenecks. *IEEE Transactions on Intelligent Transportation Systems*, 20(7), 2448-2458.
16. Geroliminis, N., Srivastava, A., and Michalopoulos, P. (2011). A dynamic-zone-based coordinated ramp-metering algorithm with queue constraints for Minnesota's freeways. *IEEE Transactions on Intelligent Transportation Systems*, 12 (4), 1576-1586.
17. Ghods, A. H., Fu, L., and Rahimi-Kian, A. (2010). An efficient optimization approach to real-time coordinated and integrated freeway traffic control. *IEEE Transactions on Intelligent Transportation Systems*, 11(4), 873-884.

18. Gomes, G., and Horowitz, R. (2006). Optimal freeway ramp metering using the asymmetric cell transmission model. *Transportation Research Part C: Emerging Technologies*, 14 (4), 244-262.
19. Gordon, R.L., 1996. Algorithm for controlling spillback from ramp meters. *Transportation Research Record*, 1554(1), 162-171.
20. Gurobi optimizer reference manual, Version 9 (2020). Gurobi Optimization, LLC.
21. Head, L., and P. Mirchandani. RHODES-ITMS. Report AZ-SP-9701. Arizona Department of Transportation, Phoenix, 1997.
22. Hegyi, A., De Schutter, B., and Hellendoorn, H. (2005). Model predictive control for optimal coordination of ramp metering and variable speed limits. *Transportation Research Part C: Emerging Technologies*, 13 (3), 185-209.
23. Hou, Z., Xu, J. X., and Yan, J. (2008). An iterative learning approach for density control of freeway traffic flow via ramp metering. *Transportation Research Part C: Emerging Technologies*, 16(1), 71-97.
24. Jacobson, L. N., Henry, K. C., and Mehyar, O. (1989). Real-time metering algorithm for centralized control. *Transportation Research Record: Journal of the Transportation Research Board*, 1232, 17-26.
25. Karimi, A., Hegyi, A., De Schutter, B., Hellendoorn, H., and Middelham, F. (2004, June). Integration of dynamic route guidance and freeway ramp metering using model predictive control. In *Proceedings of the 2004 American Control Conference (ACC 2004)* (pp. 5533-5538).
26. Kattan, L. and Saidi, M.S., 2011. Design and Evaluation of Adaptive Coordinated Ramp Control Strategies on Deerfoot Trail Using Paramics Microsimulation.
27. Kotsialos, A., Papageorgiou, M., Mangeas, M., and Haj-Salem, H. (2002). Coordinated and integrated control of motorway networks via non-linear optimal control. *Transportation Research Part C: Emerging Technologies*, 10(1), 65-84.
28. Li, Z., Chang, G. L., and Natarajan, S. (2009). An integrated off-ramp control model for freeway traffic management. Presented at 15th World Congress on Intelligent Transportation Systems, New York.
29. Li, Z., Liu, P., Xu, C., Duan, H., and Wang, W. (2017). Reinforcement learning-based variable speed limit control strategy to reduce traffic congestion at freeway recurrent bottlenecks. *IEEE Transactions on Intelligent Transportation Systems*, 18 (11), 3204-3217.
30. Lim, K., Kim, J. H., Shin, E., and Kim, D. G. (2011). A signal control model integrating arterial intersections and freeway off-ramps. *KSCE Journal of Civil Engineering*, 15(2), 385-394.
31. Lipp, L.E., Corcoran, L.J. and Hickman, G.A., 1991. Benefits of central computer control for Denver ramp-metering system (No. 1320).
32. Liu, H. X., Wu, X., & Michalopoulos, P. G. (2007). Improving queue size estimation for Minnesota's stratified zone metering strategy. *Transportation research record*, 2012(1), 38-46.
33. Liu, J. C. S., Kim, J. L., Chen, Y., Hao, Y., Lee, S., Kim, T., and Thomadakis, M. (1994). An Advanced real-time ramp metering system (ARMS): the system concept. Texas Transportation Institute.
34. Liu, Y., Chang, G. L., and Yu, J. (2011). An integrated control model for freeway corridor under nonrecurrent congestion. *IEEE Transactions on Vehicular Technology*, 60(4), 1404-1418.
35. Lu, Y., Yang, X., & Chang, G. L. (2014). Algorithm for detector-error screening on basis of temporal and spatial information. *Transportation Research Record*, 2443(1), 40-48.
36. Masher, D. P., Ross, D. W., Wong, P. J., Tuan, P. L., Zeidler, H. M., and Petracek, S. (1975). Guidelines for design and operation of ramp control systems.
37. Paesani, G.F., 1997. System wide adaptive ramp metering in southern California. In *ITS America 7th Annual Meeting and Exposition: Merging the Transportation and Communications Revolutions* Intelligent Transportation Society of America (ITS America).

38. Papageorgiou, M., Blosseville, J. M., and Haj-Salem, H. Modelling and real-time control of traffic flow on the southern part of Boulevard Périphérique in Paris: Part II: Coordinated on-ramp metering. *Transportation Research Part A: General*, 24(5), 361-370, 1990
39. Papageorgiou, M., Hadj-Salem, H., and Blosseville, J. M. (1991). ALINEA: A local feedback control law for on-ramp metering. *Transportation Research Record: Journal of the Transportation Research Board*, 1320(1), 58-67.
40. Papageorgiou, M., Hadj-Salem, H., and Middelham, F. (1997). ALINEA local ramp metering: Summary of field results. *Transportation Research Record: Journal of the Transportation Research Board*, 1603(1), 90-98.
41. Papamichail, I., Kotsialos, A., Margonis, I., and Papageorgiou, M. (2010a). Coordinated ramp metering for freeway networks – a model-predictive hierarchical control approach. *Transportation Research Part C: Emerging Technologies*, 18 (3), 311-331.
42. Papamichail, I., Papageorgiou, M., Vong, V., and Gaffney, J. (2010b). Heuristic ramp-metering coordination strategy implemented at Monash freeway, Australia. *Transportation Research Record: Journal of the Transportation Research Board*, 2178 (1), 10-20.
43. Pasquale, C., Sacone, S., Siri, S., and De Schutter, B. (2017). A multi-class model-based control scheme for reducing congestion and emissions in freeway networks by combining ramp metering and route guidance. *Transportation Research Part C: Emerging Technologies*, 80, 384-408.
44. Piotrowicz, G., and Robinson, J., 1995. Ramp Metering Status in North America. Federal Highway Administration, FHWA (No. DOT-T-95-17).
45. Pranevičius, H., & Kraujalis, T. (2012). Knowledge based traffic signal control model for signalized intersection. *Transport*, 27(3), 263-267.
46. PTV VISSIM 10 user manual (2018). PTV AG: Karlsruhe, Germany.
47. Schrank, D., Albert L., Eisele B., and Lomax, T. (2021) 2021 Urban Mobility Report. Texas A&M Transportation Institute.
48. Smaragdis, E., and Papageorgiou, M. (2003). Series of new local ramp metering strategies: Emmanouil smaragdis and markos papageorgiou. *Transportation Research Record: Journal of the Transportation Research Board*, 1856(1), 74-86.
49. Smaragdis, E., Papageorgiou, M., and Kosmatopoulos, E. (2004). A flow-maximizing adaptive local ramp metering strategy. *Transportation Research Part B: Methodological*, 38(3), 251-270.
50. Su, D., Lu, X.Y., Horowitz, R. and Wang, Z., 2014. Coordinated ramp metering and intersection signal control. *International Journal of Transportation Science and Technology*, 3(2), 179-192.
51. Sun, X. and Horowitz, R., 2005, June. A localized switching ramp-metering controller with a queue length regulator for congested freeways. In *Proceedings of the 2005 American Control Conference*, 2141-2146, IEEE.
52. Tian, Z., Messer, C., Balke, K., and Urbanik, T. (2005). Integration of diamond interchange and ramp metering operations. *Transportation research record*, 1925(1), 100-111.
53. Tian, Zongzhong (2007). Modeling and implementation of an integrated ramp metering-diamond interchange control system. *Journal of Transportation Systems Engineering and Information Technology*, 7(1), 61-69.
54. Wang, Y., Perrine, K.A. and Lao, Y., 2008. Developing an area-wide system for coordinated ramp meter control (No. TNW2008-11). *Transportation Northwest (Organization)*.
55. Wang, S., Xu, J., & Luo, Q. (2012, July). Study on on-ramp control strategy of urban freeway based on fuzzy control. In *Proceedings of the 10th World Congress on Intelligent Control and Automation* (pp. 2512-2516). IEEE.
56. Wang, Y., and Papageorgiou, M. (2006). Local ramp metering in the case of distant downstream bottlenecks. In *Proceedings of IEEE Intelligent Transportation System Conference*, 426-431.

57. Wattleworth, J.A., 1965. Peak-period analysis and control of a freeway system (No. Hpr 1/4). Texas Transportation Institute.
58. Wu, C.J., Lu, X.Y., Spring, J. and Horowitz, R., 2018, January. Field Test Implementation of Coordinated Ramp Metering Control Strategy: A Case Study on SR-99N. In Transportation Research Board Meeting 96th Annual Meeting.
59. Xu, J., Yu, W. S., and Wang, F. Y. (2006). Ramp metering based on adaptive critic designs. In 2006 IEEE Intelligent Transportation Systems Conference, 1531-1536.
60. Yang, X., Cheng, Y., and Chang, G. L. (2018). Integration of adaptive signal control and freeway off-ramp priority control for commuting corridors. *Transportation Research Part C: Emerging Technologies*, 86, 328-345.
61. Yang, X., Lu, Y., and Chang, G. L. (2014). Dynamic signal priority control strategy to mitigate off-ramp queue spillback to freeway mainline segment. *Transportation Research Record: Journal of the Transportation Research Board*, 2438(1), 1-11.
62. Zeng, X., Zhang, Y., Balke, K. N., & Yin, K. (2014). A real-time transit signal priority control model considering stochastic bus arrival time. *IEEE Transactions on Intelligent Transportation Systems*, 15(4), 1657-1666.
63. Zhang, M., Kim, T., Nie, X., Jin, W., Chu, L. and Recker, W., 2001. Evaluation of on-ramp control algorithms. California PATH Research Report UCB-ITS-PRR-2001-36. Berkeley, Calif., 2001.
64. Zhang, H. M., and Ritchie, S. G. (1997). Freeway ramp metering using artificial neural networks. *Transportation Research Part C: Emerging Technologies*, 5(5), 273-286.
65. Zhao, D., Bai, X., Wang, F. Y., Xu, J., and Yu, W. (2011). DHP method for ramp metering of freeway traffic. *IEEE Transactions on Intelligent Transportation Systems*, 12(4), 990-999.
66. Zhao, J., and Liu, Y. (2016). Integrated signal optimization and non-traditional lane assignment for urban freeway off-ramp congestion mitigation. *Transportation Research Part C: Emerging Technologies*, 73, 219-238.